

How Crystalline is Low-Density Amorphous Ice?

Michael Benedict Davies,^{1,2} Alexander Rosu-Finsen,³ Christoph G. Salzmann,^{3, a)} and Angelos Michaelides^{2, 1, b)}

¹⁾*Department of Physics and Astronomy, University College London, WC1E 6BT, UK.*

²⁾*Yusuf Hamied Department of Chemistry, University of Cambridge, Lensfield Road, Cambridge CB2 1EW, UK.*

³⁾*Department of Chemistry, University College London, 20 Gordon Street, London WC1H 0AJ, UK.*

Low-density amorphous ice (LDA) is one of the most common solid materials in the Universe and a key material for understanding the many famous anomalies of liquid water. Yet, despite its significance and its discovery dating nearly 90 years, the structure of LDA is debated. It is unclear if LDA is a glassy state representing a liquid or a heavily disordered crystal; indeed, two forms (LDA-I and LDA-II) have been discussed as amorphous and partially crystalline in the literature, respectively. Here, with two widely used water models, we show that the experimental structure factor of LDA is best reproduced computationally by a partially crystalline structure. Models for both LDA-I and LDA-II are highly similar, with differences only due to subtle differences in crystallinity and/or experimental error. Further support for this structural model of LDA comes from experiment: if LDA is partially crystalline, then its route to formation should result in different nanocrystallite cubicities, and thus give rise to different cubicities upon recrystallisation. This memory effect of LDA’s creation route is observed and it is incompatible with a fully amorphous material. The results present a unified computational and experimental view that LDA is not fully amorphous but instead a partially crystalline material. This impacts LDA’s many roles in nature and potentially our understanding of liquid water. Furthermore, the “re-identification” of such an intensely studied material highlights that great care will be needed when classifying the nature of glassy materials going forward.

I. INTRODUCTION

The matrix of life, the universal solvent, a powerful corrosive, and the strangest fluid – these are just some of the names for perhaps the most fascinating and important substance in nature: water. It is the many anomalies of water – over 70 have been compiled¹ – that facilitate its multitude of names and moreover shape the face of the Earth. Yet, despite intensive research efforts dating back to antiquity, a complete understanding of water remains a challenge. There are many physical states that water can exist in; for instance, 20 polymorphs of ice have now been created in the laboratory.^{2–7} Of all water’s forms, the most abundant in the Universe is found in the dense molecular clouds from which stars and planets are born, and as the bulk matter in comets: low-density amorphous ice (LDA).^{8,9} LDA is of great scientific interest, in part due to its involvement in cosmological phenomena (including a possible role in the origin of life¹⁰), but also due to its potential key role in explaining water’s anomalies. Specifically, whether LDA has a corresponding liquid state is a cornerstone of the heavily debated two-state liquid model, which could account for many of water’s thermodynamic anomalies.^{11–21}

The name of LDA originates from the fact that its density of 0.94 g cm^{-3} is lower than the 1 g cm^{-3} of liquid water, and because it appears to be an amorphous solid according to diffraction studies.²² However, despite

the importance of LDA, there is ambiguity with respect to its structural nature with some studies pointing towards a more “crystal-like” nature than a purely glassy state.^{13,14,16,23–28} Multiple experimental avenues for creating LDA have been discovered.^{8,22,29–39} And it is identified on the basis of broad features in diffraction. However, discerning the exact local structural nature of LDA from diffraction patterns is problematic. Amann-Winkel et al. distinguished three scenarios which are of interest for diffraction patterns of amorphous ice: a purely amorphous material, grains of crystalline ice embedded in an amorphous matrix, and a completely polycrystalline material.⁴⁰ The structural nature of LDA is further complicated by subtle differences that can be exhibited by samples depending on their preparation route (for example, LDA-I, LDA-II and LDA(ice VIII)^{41,42}). Using neutron and X-ray diffraction respectively, Finney et al. and Mariedahl et al. found the first coordination shell of LDA is similar to hexagonal ice;^{43,44} however, at longer ranges the similarity drops. It remains unclear what structural model of LDA can best explain this.

Computer simulation can provide the atomic scale resolution needed to determine the structure of LDA. A common way to obtain LDA in simulation is to quench liquid water rapidly to avoid crystallisation. Martelli et al. quenched the TIP4P/2005 water model with a cooling rate (κ) of 1 K ns^{-1} to obtain LDA samples. They searched the LDA model for crystal-ice domains in the second coordination shell and found none, concluding it was indeed fully amorphous.⁴⁵ Furthermore, by quantifying the large-scale density fluctuations they showed it was nearly hyperuniform.⁴⁶ However – as discussed by Limmer and Chandler,¹⁷ and others^{47–50} – κ

^{a)}Electronic mail: c.salzmann@ucl.ac.uk

^{b)}Electronic mail: am452@cam.ac.uk

is a key parameter which when varied affects the structural and energetic properties of water glasses. A range of different amorphous LDA samples is thus achievable in simulation. Evidence of multiple configurations corresponding to LDA have also been observed via decompression or heating high-density amorphous ice (HDA).^{51–53} Moreover, given the suggestions of a crystal-like structure in experiment, whether these fully amorphous states achievable in simulation are the best model for the LDA achieved in experiment (and detected in nature) is a key question to resolve.

In this work, we establish the structure of experimental LDA using computational and experimental approaches. Agreement with the structure factor, $S(Q)$, of LDA – as measured using wide-angle X-ray scattering of LDA-I and LDA-II by Mariedahl et al. (2018) and (2019)^{44,54} – is screened across a range of computational models obtained from two diametrically opposed pathways: (i) quenching liquid water at different κ ; and (ii) constructing large-scale polycrystalline ice structures using Voronoi domains followed by structural relaxation. In the former, the structure of LDA is explored starting from the disordered liquid water state, whilst in the latter it is approached using ordered crystalline ice building blocks. For optimal accuracy, we consider stacking disorder in the building blocks. And computationally large system sizes (on the order of 190,000 – 320,000 water molecules) are employed to better enable capturing the short-range order vs. long-range anisotropy in polycrystalline systems. Experimentally, we investigate the crystallisation products of different types of LDA with respect to stacking disorder. The aim is to search for memory effects: these are expected if LDA is partially crystalline but not if it is fully amorphous.

II. RESULTS

A. Quenching liquid water indicates that LDA-I and LDA-II are partially crystalline states.

To begin, we performed molecular dynamics simulations in which liquid water, represented by the mW water model,⁵⁵ was quenched from 300 K to 125 K (see *Methods*). Depending on the cooling rate (κ) a wide variety of amorphous ice materials was obtained, ranging from partially crystallised states to polycrystalline (almost fully crystallised) states, as shown in Fig. 1 a. The former are observed for $\kappa \geq 5 \text{ K ns}^{-1}$, and resemble multiple isolated grains of crystalline ice embedded within an amorphous matrix. The latter is obtained with $\kappa = 1 \text{ K ns}^{-1}$, and resembles multiple grains of ice packed together. The formation of these various structures simply comes down to a competition of timescales between water diffusion and ice crystallisation. The key question is which, if any, of these amorphous and partially crystalline states is a good model for LDA?

To help answer this, we report in Fig. 1b the struc-

ture factors of the quenched systems alongside experimental measurements of LDA. In experiment, Winkel et al. reported the existence of two sub-states of LDA – which they named LDA-I and LDA-II – that exhibit subtle structural differences in their diffraction patterns.⁴¹ It has been suggested that LDA-I may contain crystalline ice whilst LDA-II does not on the basis of crystallisation temperatures.^{28,56} We therefore compare the X-ray diffraction pattern of LDA-II collected by Mariedahl et al. (2018)⁴⁴ and the X-ray diffraction patterns of LDA-I by Mariedahl et al. (2019)⁵⁴ to our computational models.

Fig. 1b shows that the optimal structural model for both LDA-I and LDA-II is a partially crystalline state – yet with stacking-disordered ice – present in numerous and diversely sized grains. Interestingly, agreement with the experimental data is observed to be a “goldilocks” scenario with the best model being not too amorphous and not too crystalline. The key effect of crystallinity in these states is on the prominence of the first peak and trough in $S(Q)$, which reflects more long-range structural characteristics compared to the higher Q features. The nucleation rate has a per unit time and per unit volume dependence, and these dependencies can physically explain the states achieved from quenching: the former explains the effect of κ ; the latter is captured by system size. Fig. S1 shows that smaller systems give poorer matches to LDA as a result of the reduced length scale impairing the ability to capture polycrystalline structures. The proportion of cubic (c) local environments in stacking disordered ice I – termed the “cubicity” – in the ice grains is 48 %, which is close to the expected 50 % cubicity obtained in homogeneous ice nucleation.^{57–61}

To quantify the agreement between the computational models and experiment the Pendry R-factor (R) was employed⁶² over the experimental Q range of $1.0 - 23 \text{ \AA}^{-1}$. R was developed and is widely used in low-energy electron diffraction to quantify the agreement of computational models with experimental data (see *Methods*). A value of $R = 0$ represents perfect agreement whereas values of ≈ 0.1 are taken as excellent, ≈ 0.2 as good, ≈ 0.3 as mediocre, and ≈ 0.5 as bad.⁶³ Fig. 1c shows that the three partially crystallised states have excellent agreement with experiment. The best models for LDA-I and LDA-II are the systems with 13 % and 19 % crystalline ice, respectively. The respective R values are 0.025 and 0.021, which indicate extremely high agreement. Fig. S2 shows qualitative agreement between R and the coefficient of determination. Fig. S3 shows $S(Q)$ for the best LDA model and experimental data over the full $0.65 - 23 \text{ \AA}^{-1}$ range.

Our results suggest that LDA-I and LDA-II are both partially crystalline states, containing stacking disordered ice. Furthermore, we find that the optimal match for LDA-I is slightly less crystalline than that found for LDA-II – in contrast to the suggestion in literature that LDA-I contains crystallites whereas LDA-II does not (on the basis of crystallisation temperatures). To investigate

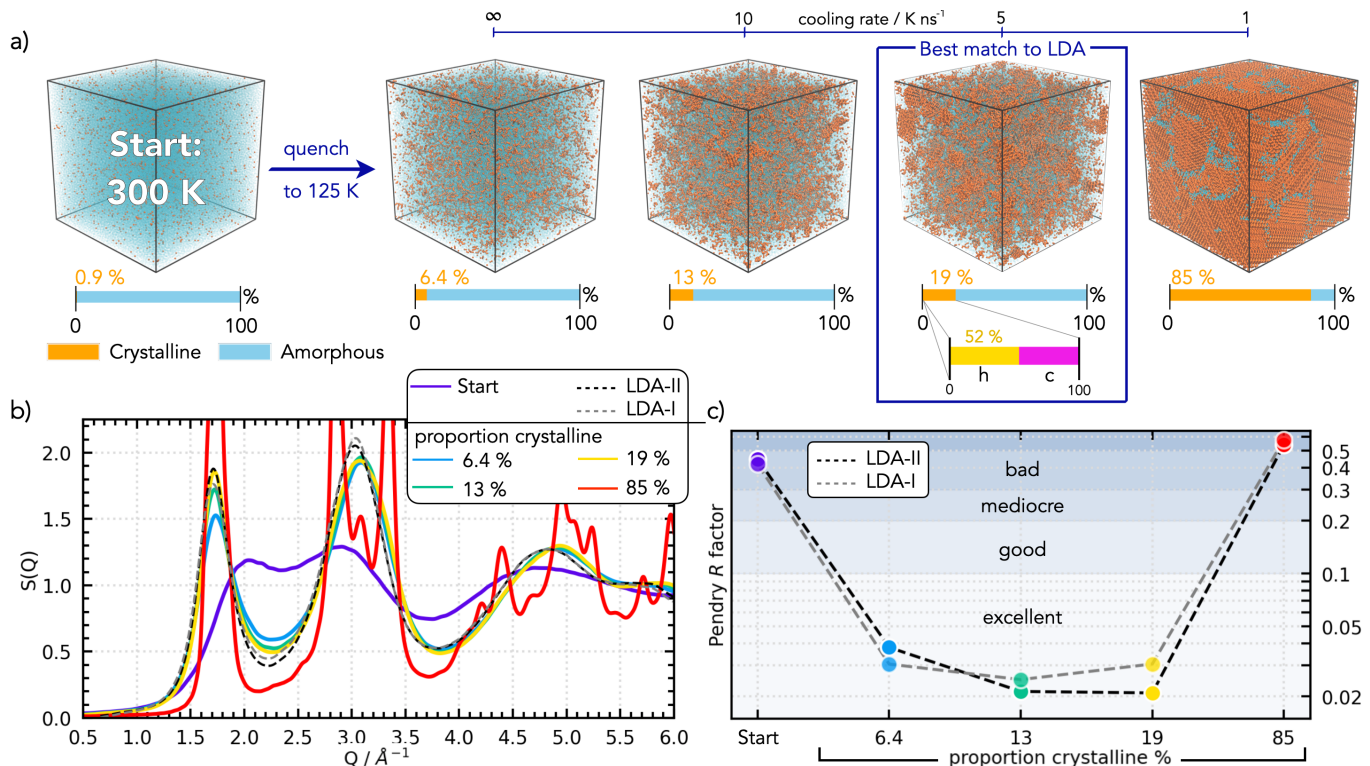


FIG. 1. **Quenching liquid water: the experimental diffraction data of LDA is best modelled with a partially crystalline state.** (a) Snapshots of systems taken from quenching water from 300 K to 125 K at different cooling rates. “Start” indicates equilibrated water at 300 K and ∞ K ns $^{-1}$ indicates immediate cooling to 125 K. (b) $S(Q)$ of the quenched systems along with experimental data of LDA-II from ref. 44 and LDA-I from ref. 54 (c) Pendry R factor (of the agreement between experiment and theory) against crystallinity of structure achieved in quenching. The proportion of hexagonal (h) and cubic (c) local environments are indicated for the best model in (a).

this further, Fig. S3 shows an LDA-I diffraction pattern along with two different experimental measurements of LDA-II. The LDA-I data lies within the variation of the two different LDA-II measurements. This suggests the difference between LDA-I and LDA-II may be within experimental error. Furthermore, in Raman spectroscopy no difference could be found between LDA-I and LDA-II.⁶⁴ In conclusion, we find LDA-I and LDA-II are both similar partially crystalline states, with any structural differences between LDA-I and LDA-II due to subtle differences in crystallinity, experimental error or both. Given this, the rest of this study employs the LDA-II experimental sample of ref. 44 as “LDA” for the sake of brevity.

B. LDA is optimally modelled as a partially crystalline state by both the mW and TIP4P/2005 water models.

We next extended the analysis by applying the same quenching protocol to the atomistic TIP4P/2005 water model.⁶⁵ In Fig. 2, we show that TIP4P/2005 and mW optimally model experimental LDA as a partially crystalline state. TIP4P/2005 follows the same pattern as mW, displaying an improved match to LDA as the

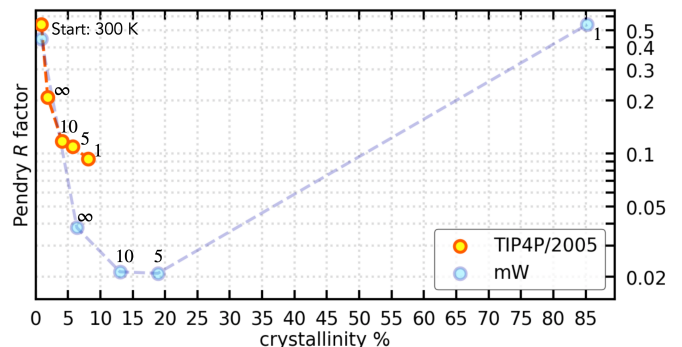


FIG. 2. **Quenching two water models indicates LDA is a partially crystalline state.** Pendry R factor of experimental LDA against percentage crystallinity of computational model, for the TIP4P/2005 and mW water models, as obtained by the quenching procedure detailed in Fig. 1. Data points are labelled with the employed cooling rate (κ).

proportion of crystallinity increases from 1.9 % to 4.1 % to 5.7 % to 8.1 %. Fig. S4 show the respective system snapshots and $S(Q)$.

The slower nucleation rate and dynamics of TIP4P/2005 result in more highly amorphous states,

when subject to the same cooling ramp procedure as mW. The highest crystallinity achieved by TIP4P/2005 in the cooling ramps yielded the best match to LDA, thus 8.1 % is a lower bound estimate for LDA’s crystallinity for TIP4P/2005. The trend indicates that higher levels of crystallinity would yield even more accurate agreement, however the computational cost of obtaining this is not practical in this study due to the model’s order of magnitude increase in cost combined with the κ required (on the order of 0.01 K ns^{-1}). We refer the reader to the methods section for more discussion on the water models.

C. Models of polycrystalline ice indicate LDA is a partially crystalline state.

Next, we investigated the diametrically opposed pathway to creating LDA from liquid water; specifically, creating LDA from crystalline ice. The random arrangement of many ice grains can broaden the diffraction features of crystalline samples, yielding amorphous-like $S(Q)$. To this end, large-scale ($\approx 320,000$ water molecules) periodic polycrystalline structures with different levels of polycrystallinity and cubicity were built using Voronoi domains. The structures were subsequently geometry optimised and annealed at 125 K using the mW water model. A grid search was set up as illustrated in Fig. 3 to find the most optimal model for LDA.

Fig. 3a shows a heatmap of the R values of the relaxed polycrystalline models benchmarked against the experimental LDA $S(Q)$. A strong dependence of the agreement is seen with polycrystallinity. Fig. 3b shows this is due to the increasing amorphous nature of the diffraction patterns with increasing polycrystallinity. The “goldilocks” scenario is again observed. The optimal match is found for the 2,500 grain systems which have an optimal R value of 0.022. Both lower and higher levels of polycrystallinity (and thus proportion of crystalline versus amorphous) result in poorer matches to experiment. Fig. 3c shows the structure of the best fit. Again, the structure is a partially crystallised state with isolated grains of crystalline (yet stacking disordered) ice surrounded by amorphous “filler” regions. The amorphous regions arise during the structure relaxation due to the lattice mismatches between the various Voronoi domains. Since ice is a “soft” molecular material it yields quite thick amorphous regions at the grain boundaries. At this high level of polycrystallinity the system is 25 % crystalline and 75 % amorphous. It thus no longer resembles a “traditional” polycrystalline system – the type highlighted by Amann-Winkel et al. to be of interest but not a probable structure for amorphous ices⁴⁰ – which have sharp interfaces at the grain boundaries and are therefore primarily crystalline. A weak, but noticeable, dependency on the match to experiment is seen for the level of cubicity in Fig. 3a, with a best match around 25 – 50 %.

The two different approaches – building polycrystalline ice and quenching liquid water – converge to very similar structural models of LDA. This gives additional confidence that experimental LDA is indeed partially crystalline. The subtle differences between the two models of LDA are discussed in the SI. Here, it is sufficient to say that differences in the uniformity of grain size are the origin of the slight difference in the crystallinity.

D. Exploring the hybrid amorphous-crystalline nature of LDA.

We next further investigated the hybrid amorphous-crystalline nature of the optimal LDA models from quenching liquid water and building polycrystalline ice. In Fig. 4a the distributions of the atomic local environments of water, ice I_h , ice I_c , and the LDA models are plotted. “Local” here refers to measurements of order within the first coordination shell, as defined by local q_6 and local q_3 (see *Methods*). The local environments of the two LDA models are very similar to each other. They contain significant amounts of highly crystalline and amorphous (as explored by liquid water) atomic local environments, with a smooth distribution of environments explored between these two levels of local order.

The hybrid amorphous-crystalline nature is also reflected in the oxygen-oxygen radial distribution functions, $g(r)$, shown in Fig. 4b and c. The two LDA models have near identical $g(r)$ and both show a very good agreement to experiment, which is well maintained up to the longest range signal measured in experiment of 23 Å. In the short-range, up to ~ 6 Å the first coordination shell of LDA is very similar to crystalline ice whereas the second coordination shell is broadened. From ~ 6 Å onwards LDA’s radial correlations quickly decay leaving it dissimilar to crystalline ice; yet, the correlations remain much stronger than in liquid water. Thus, again LDA lies between the two. Mariedahl et al. (2018) made similar observations from their experimental signal, stating “it is essential to develop models of amorphous ices that can better describe these intermediate-range correlations”.⁴⁴ Similar observations were also made by Finney et al.⁴³ who found “considerable similarity in the local order between LDA and ice I_h ..., [but] beyond the second shell there are increasing discrepancies between their respective $g(r)$ ”. The strong agreement between the LDA models and experiment show this structure is accurately modelled and explained by a partially crystalline state. The anisotropically arranged grains result in short-range similarity to crystalline ice, but long-range decays in $g(r)$. The primitive ring distributions of the LDA models are shown to be very similar in Fig. S6, and are also consistent with partially crystallised states.

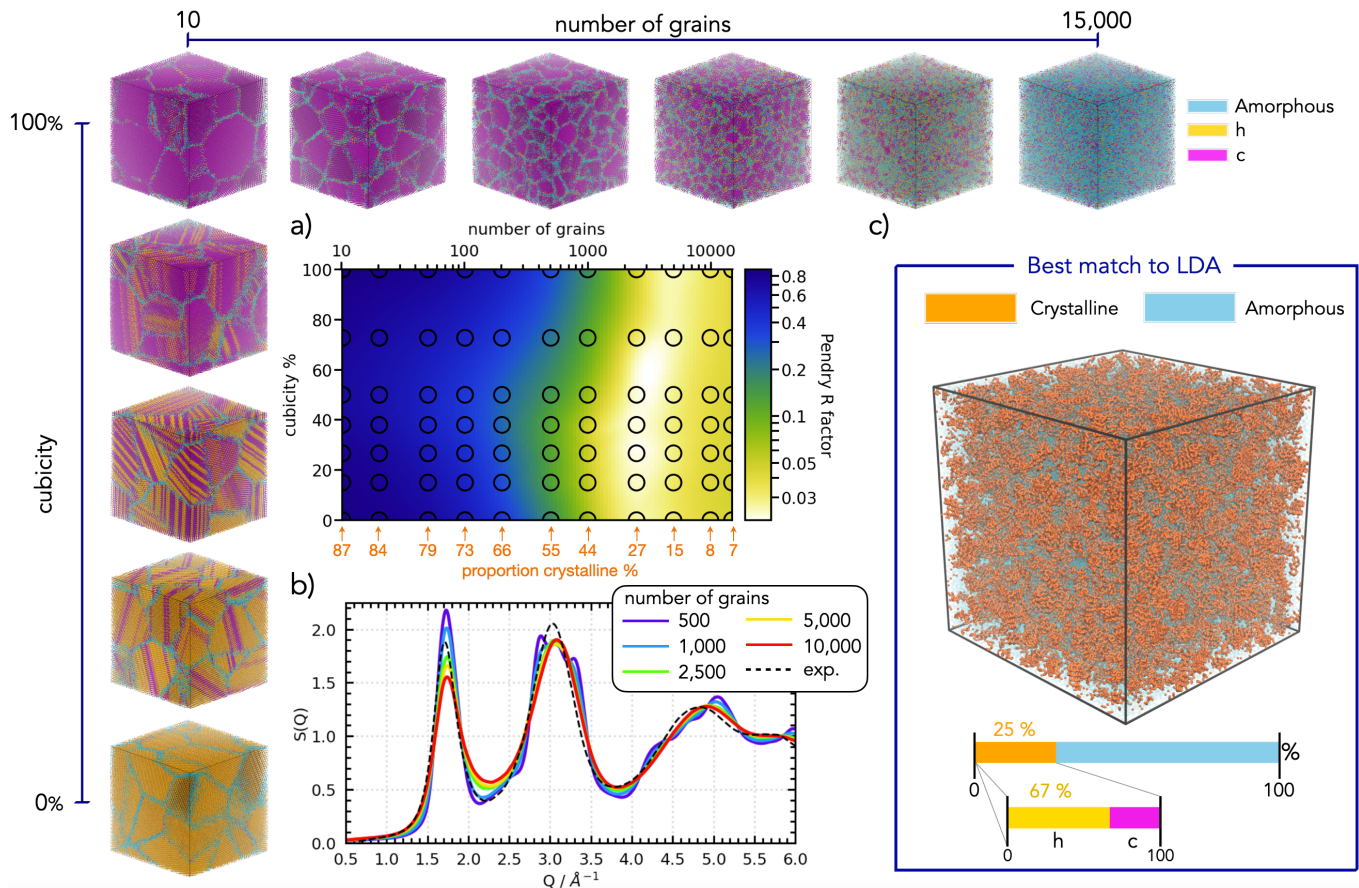


FIG. 3. **Constructing LDA with Voronoi domains containing crystalline ice.** The agreement between experiment and polycrystalline systems was explored for model systems across a grid of different levels of cubicity (of the subset of molecules in crystalline environments) and polycrystallinity (given by the number of grains). Snapshots of the grid’s top and left boundaries decorate the borders of the figure, and the approximate mean diameters of the grains are shown in Fig. S5. (a) Heatmap of the Pendry R factor for the agreement of the $S(Q)$ between experiment and the model systems and the computational systems as a function of the proportion of molecules with crystalline ice environments and the cubicity. (b) The computational $S(Q)$ with optimal agreement with experiment for different levels of polycrystallinity. (c) Snapshot of the system with the best match to the experimental data, with its local atomic environments indicated. System contains approximately 320,000 water molecules.

E. Cubicity memory effects in experimental LDA samples can be explained by a hybrid amorphous-crystalline state.

Experimentally, we found indirect evidence for the presence of crystallinity in LDA by heating it to form stacking disordered ice (ice I_{sd}) and quantifying the stacking probabilities. Fig. 5 shows a remarkable variability in the stacking probabilities of ice I_{sd} obtained from differently prepared LDA samples. Each LDA sample has a different “parent” phase: unannealed high-density amorphous ice (uHDA) formed by compressing ice I_h , ice I_{sd} and medium density amorphous ice (MDA) respectively;⁶⁶ expanded high-density amorphous ice (eHDA) formed by heating a compressed sample of uHDA; ice VIII; vapour deposition to give amorphous solid water (ASW); and the hyperquenching, performed by Kohl et al. in ref. 67, of an aerosol of liquid water droplets to give hyperquenched glassy water (HGW).

A fully amorphous LDA structure should not display

memory effects with respect to the parent phase. Instead, nucleation occurring from a fully amorphous structure would follow homogeneous nucleation, which results in random stacking with 50 % cubicity.^{57–61} However, the obtained cubicities here range from 20 – 65 %. This indicates that that crystal growth from already existing ice I_{sd} seeds is the dominant process, not homogeneous nucleation. In summary, if LDA is partially crystalline, then the route to formation can be expected to potentially result in different nanocrystallite cubicities, and thus give rise to different cubicities upon recrystallisation. This is observed. A fully amorphous material would not display such memory effects.

The relatively weak dependence of cubicity – observed earlier in the polycrystalline LDA models – shows that crystalline ice I grains with different cubicities can be well hidden in the broad diffraction features of LDA samples. Similar differences in the crystallisation behaviour of LDA samples created via different pathways have also

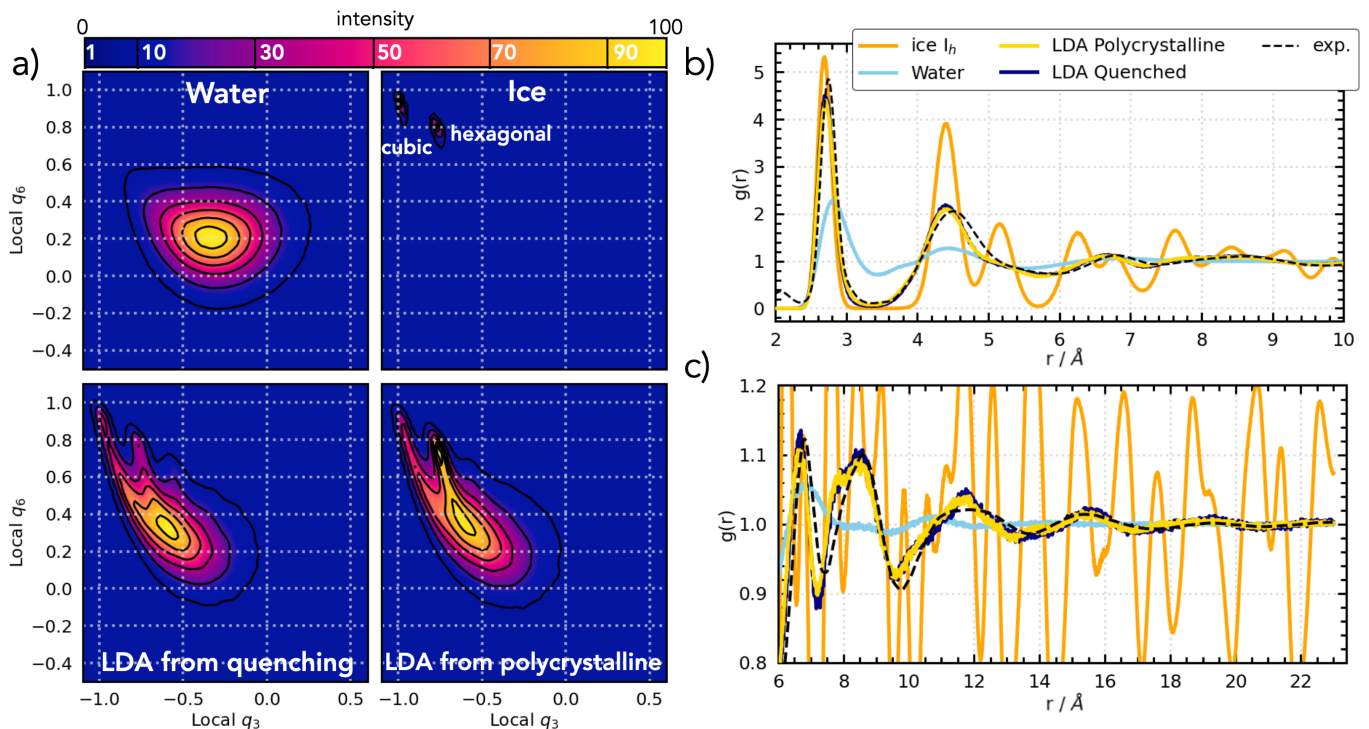


FIG. 4. **The hybrid amorphous-crystalline nature of LDA.** (a) Probability densities of the local atomic environment of water, ice, and the LDA models. Contours are drawn at 90, 70, 50, 30, 10, and 1 % of the height of the respective probability densities. (b) & (c) Oxygen-oxygen radial distribution functions at short (b) and long (c) range for the computational models and experiment. Ice I_h , ice I_c and the LDA models are sampled at 125 K and water at 250 K.

been reported by Seidl et al.⁵⁶ and Mariedahl et al.⁵⁴ – but accurate cubicities have not been reported.

III. DISCUSSION

In this work, we present a combined computational and experimental approach showing that LDA has a hybrid amorphous-crystalline structure. Computational models with near exact agreement of the structure factors with experiment were achieved through multiple modelling approaches. The quenching of liquid water – both with the mW and TIP4P/2005 water models – optimally modelled LDA as a partially crystalline state. And building polycrystalline ice systems – a diametrically opposed pathway to quenching – also optimally modelled LDA as a partially crystalline state. In all cases, matching experiment was found to be a “goldilocks” scenario, where the structure is not too amorphous and not too crystalline. The models resemble a partially crystalline state with grains of stacking disordered crystalline ice surrounded by amorphous “filler regions”. Experimentally, indirect evidence of LDA’s hybrid amorphous-crystalline state was found by transforming LDA to ice I_{sq} : a memory effect with respect to the parent material of LDA is seen in the stacking probabilities that cannot be explained by a fully amorphous LDA state and hence indicates the presence of crystalline ice grains already in the LDA with different

cubicities.

Finney et al. estimated that any crystallites in LDA were less than 15 \AA ,⁴³ and used this to suggest ruling out a partially crystalline structure of LDA. Instead, we find that a partially crystalline structure is indeed the optimal model for LDA, as it provides the required short-scale local crystalline structure but long-scale homogeneity. The distribution of many (anisotropically arranged) small crystallites has been discovered to be essential to modelling LDA. The resulting structure is far from a fully amorphous material: both at the local- (individual crystallites) and global-scale ($\approx 25\%$ crystalline). The system snapshots in Fig. 1 and 3 perhaps best illustrate this partially crystalline nature. An estimate for the diameter of the grains in these systems is provided in Fig. S5. We find the optimal model system, containing 2,500 grains, has a mean grain diameter of 25 \AA . The crystalline sizes are subject to stochastic variation. Therefore, using the grain sizes from the next nearest models to the optimal, we suggest crystallites in LDA will range from 30 – 15 \AA in size. It is worth noting, Finney et al. considered only ice I_h crystallites and did not consider for stacking disorder, as done here, which has a broadening effect on diffraction features.

The mW water model enabled the discovery of the optimal models, as its computational cost and dynamics enabled the system sizes and time scales required to capture the partially crystalline systems. mW has been

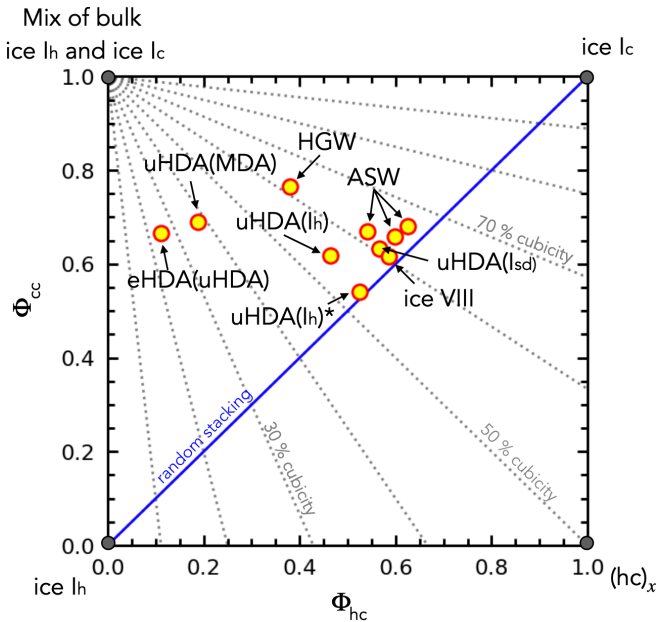


FIG. 5. **Experimental stacking probabilities of ice I_{sd} obtained from LDA depend on how the LDA was made.** In this “stackogram”, Φ_{cc} and Φ_{hc} define the probabilities of cubic stacking after a previous cubic or hexagonal stacking event, respectively. The blue diagonal line represents random stacking, where Φ_{hc} and Φ_{cc} are equal. The dashed grey lines indicate constant cubicities. The four corners represent ice I_h , ice I_c , a physical mixture of the two and the $(hc)_x$ polytype which consists of strictly alternating cubic and hexagonal layers of ice. For each data point the “parent” phase from which the LDA was made is noted. For uHDA and eHDA the “grandparent” phases are also given in brackets. uHDA(I_h)* was created using a different experimental procedure to the other uHDA samples (see *Methods*).

widely and successfully employed to study water, crystalline ice and amorphous ice. And has been specifically shown to accurately model low-pressure states of ice, including LDA.⁵⁵ However, it is a coarse-grained model meaning it has inherent limitations such as the ability to distinguish between acceptors and donors of hydrogen bonds. We therefore also employed the atomistic TIP4P/2005 water model, a well regarded classical water model that has been extensively used to model amorphous ice. TIP4P/2005 also optimally modelled LDA as partially crystalline. The increased cost meant more highly crystalline structures were not feasible to obtain; however, it was shown to be at least 8% stacking disordered crystalline ice, with a clear trend to indicate the optimal models would have higher crystallinity. Two widely used and disparate water models have thus been shown in this study to optimally model experimental LDA as a partially crystalline state. Looking to the future, extending the analysis to machine learned force-fields for water is desirable. However, the time scales and system sizes necessary are far beyond current feasible computational costs at present.

Different preparation routes yield different nomenclatures for LDA in the literature. Of particular importance to this study is LDA-I and LDA-II, since they had been suggested to be two distinct sub-states of LDA.^{28,56} We found that both LDA-I and LDA-II are accurately modelled as similar partially crystalline states. Any difference between the two likely comes from experimental error, and/or potentially subtle differences in crystallinity and/or cubicity. Moreover, if LDA is a partially crystalline material then different preparation routes should lead to potentially different cubicities in the nanocrystallites, and thus different behaviours upon crystallisation to ice I. This is observed experimentally (over seven different formation routes to LDA) and thus provides evidence that the many different nomenclatures of LDA in the literature are indeed partially crystalline materials.

In addition to experimental X-ray diffraction results, the very similar local environments in LDA and ice I presented here are also consistent with their Raman spectra of their O-H stretching modes.⁶⁸ In fact, the LDA to ice I_{sd} phase transition is barely visible in Raman spectroscopy. Moreover, the very small downshift observed in the O-H stretching modes upon crystallisation is consistent with strain release. Such strain release would occur between the anisotropically strained ice grains in LDA due to the lattice mismatch between neighbouring grains. The strain is released when LDA crystallises to ice I_{sd} as the ice grains grow larger, coalesce and align in orientation. In Fig. S7, the vibrational density of states for the different levels of polycrystallinity explored in this study are plotted. This shows a qualitative agreement with experiment whereby the spectra show a weak dependence on the level of polycrystallinity and no dependence on the cubicity.

A hybrid-crystalline structure of LDA has potential wide-reaching implications. Being the most abundant form of water in the universe, LDA is important in astronomy; for instance, in astrochemistry LDA is thought to play a key role in promoting the variety, complexity and richness of molecules observed in the stellar-forming regions of space.^{9,10} In cryopreservation, the vitrification (avoidance of ice crystallisation) of biological matter is thought to be key to cell survival – here a fully amorphous LDA is desired to act as the embedding matrix.^{69,70} A fully amorphous LDA is similarly desired in the widely used technique of cryogenic electron microscopy⁷¹ – achieving a truly amorphous LDA would help prevent sample damage and improve resolution. Crucially, LDA is key for our understanding of liquid water. A corresponding liquid state to LDA is central to the two-state model. And whilst a fully amorphous LDA can be achieved in simulation, confirming if a fully amorphous LDA can be achieved experimentally or exists in nature is now of paramount importance – especially given the recent discovery of MDA.⁶⁶ To achieve a fully amorphous LDA, novel techniques might need to be employed. For instance, a rapid enough cooling rate might completely avoid crystallisation.

Finally, the findings of this study have implications for the structural nature of other amorphous materials. The other amorphous ices, such as HDA, are of immediate interest. As are the myriad of glasses that underpin many technologies (for example, OLEDs and fibre optics). The beneficial application of glasses over crystals is largely due to their macroscopic homogeneity and absence of grain boundaries.⁷² Determining whether materials are truly glassy or not could provide future opportunities for technological innovation. Indeed, in the literature it has already been shown that amorphous silicon can be equally well modelled by a partially crystalline structure instead of one that is fully amorphous.^{73,74} Another question that arises is the nature of “ultrastable glasses”^{72,75} – a class of material that can exhibit highly desirable properties. The low entropy of these materials could be explained by the presence of crystalline grains that were previously undetected, thereby providing a resolution to the Kauzmann paradox.⁷⁶

IV. METHODS

A. Molecular dynamics (MD) simulations.

MD simulations were performed with the large-scale atomic/molecular massively parallel simulator (LAMMPS) code.⁷⁷ Cubic simulation boxes periodic in x , y , z were used. The constant number of molecules, constant pressure, and constant temperature (NPT) canonical ensemble was sampled using 10-fold Nosé-Hoover thermostats and barostats. MD simulations of mW used thermostats and barostats with relaxation times of 500 femtoseconds (fs) and 5 picoseconds (ps) respectively, and integrated the equations of motion with a timestep of 10 fs. MD simulations of TIP4P/2005 used thermostats and barostats with relaxation times of 200 fs and 2 ps, respectively. Simulations of quenching liquid water and of annealing polycrystalline ice employed isotropic and anisotropic barostats, respectively.

There are, of course, many water models. In this study we chose to use mW because it offers the best trade-off between accuracy and computational cost. The choice was based on several reasons: (i) mW accurately captures important properties of water such as the density, structure, melting temperature, and the formation of LDA;⁵⁵ (ii) it has been widely and successfully used in studying the nucleation of ice;^{55,60,61,78–83} (iii) it accurately captures the metastability of ice I_c ^{55,84} as well as the thermodynamics of stacking faults;^{60,85,86} (iv) crucially, because it is considerably cheaper than an all-atom model and has faster dynamics mW enables quenching and crystallisation simulations in large system sizes ($> 100,000$ particles) – such system sizes are essential for determining the balance of ice-like and amorphous domains. The TIP4P/2005 water model was employed as an atomistic water model as it has also been widely and successfully applied to study water and ice, including the formation

of LDA.^{19,45,46,65,81,87}

Quenching simulations were performed in a similar fashion to Gartner et al.⁵⁰ Water was first equilibrated at 300 K and 0 Pa for 2 ns, prior to generating starting configurations. The desired κ rate was achieved by smoothly ramping the temperature from 300 K to 125 K over the required time period. For $\kappa = \infty$ K/ns, the structure was further relaxed (4 ns for mW, and 20 ns for TIP4P/2005).

Using our Stacky program,⁸⁸ a range of ice I supercell structures with 60 layers, 322,560 mW water molecules and cubicities of 1, 0.73, 0.5, 0.37, 0.27, 0.13 and 0 were produced. After transforming the hexagonal to orthorhombic cells, the cell dimensions were 21.5, 21.8 and 22.0 nm in x , y , z . The purpose-written nanoVD program then used these structures to create 5, 10, 20, 50, 100, 200, 500, 1,000, 2,500, 5,000, 10,000 or 15,000 Voronoi domains within a cell of the same size. The center points of the Voronoi domains were randomly chosen. The ice I structures were rotated randomly using a zyz rotation matrix and shifted by random fractions of the cell edges. The latter step is essential to ensure that the final polycrystalline structure reflects the cubicity of the parent structure. The structures were then placed at the centers of the Voronoi domains followed by deleting all molecules that were more than half-way away with respect to the centers of the surrounding Voronoi domains including those located outside the cell through the periodic boundary conditions. As a quality check, it was confirmed for each polycrystalline structure that the number of the mW molecules approximately matched the corresponding number in the start structure.

The various polycrystalline structures with different domain sizes and cubicities were then geometry optimised in LAMMPS using the steepest descent algorithm, then equilibrated at 125 K and 0 Pa for 50 ps with a timestep of 0.25 fs, then for 2 ns with a timestep of 10 fs, prior to undertaking analysis. Fig. S10 shows snapshots of the systems before and after the geometry optimisation plus equilibration.

Structure factors were calculated using the Debyer software (<https://github.com/wojdyr/debyer>) with a cutoff of half the minimum box dimension, and the sinc-fuction ($\sin(x)/x$) to dampen the cut-off and reduce the Fourier termination effects. Ring statistics were calculated with the Rigorous Investigation of Networks Generated using Simulations (R.I.N.G.S) software⁸⁹ and the primitive rings criterion. The Visual Molecular Dynamics software⁹⁰ was used to calculate radial distribution functions and to generate images of systems.⁹¹

B. Classifying local environment of water molecules.

The local q_6 order parameter of Li et al. was used to classify mW molecules as either crystalline or amorphous.⁷⁸ The threshold for labelling a particle as crystalline or amorphous was calculated following the

methodology used by Espinosa et al.⁹² Periodic boxes of bulk ice I_h , ice I_c , and water containing 184,000, 216,000 and 192,000 mW molecules respectively were simulated at 250 K and 0 Pa, and the corresponding local q_6 values were extracted every 200 ps over 2 ns. The distribution of the local q_6 values for crystalline and amorphous environments were then taken from the bulk crystalline ice and bulk liquid water simulations respectively. As shown in Fig. S11 the cutoff for the local q_6 between crystalline and amorphous environments are then taken where the probability of mislabelling a particle as crystalline when it is amorphous and vice versa is equal: local q_6 gives a mislabelling percentage of 0.8 % here. A similar methodology was used to classify molecules as either ice I_h or ice I_c , where instead the local q_3 values were compared between bulk ice I_h and ice I_c . Fig. S12 which shows that local q_3 gives a mislabelling percentage of 0.04 % here for the mW model.

The same method was used to distinguish crystalline form amorphous molecules for the TIP4P/2005 model (using the configuration of the oxygens); however an alternative definition of local q_6 by Lechner and Dellago⁹³ was used as it was found to give a smaller mislabelling percentage here than that of Li et al. Fig. S13 shows a mislabelling percentage of 0.84 % was achieved.

The plugin for metadynamics 2 (PLUMED2)^{94,95} was used to calculate local q_6 and local q_3 .

C. Pendry R-factor.

The Pendry reliability factor (“Pendry R-factor”) was calculated as defined by Pendry.⁶² Let f be a signal and \dot{f} be its first derivative. To compare f with another signal, the logarithmic derivative is employed to give emphasis on the location of the maxima/minima rather than the amplitudes.

$$L = \dot{f}/f \quad (1)$$

A comparison between theory, \bar{L} , and experiment, \hat{L} , using the L functions gives too high an emphasis to zeros; therefore, the Pendry y-function is then employed to give a similar emphasis to troughs and peaks in the signal

$$Y = L^{-1}/(L^{-2} + V^2) \quad (2)$$

The imaginary part of the electron self energy term used in the LEED community, V , was set to two here. The Pendry R factor between theory, \bar{Y} , and experiment, \hat{Y} , is then defined as

$$R = \frac{\sum_i (\bar{Y}_i - \hat{Y}_i)}{\sum_i (\bar{Y}_i^2 + \hat{Y}_i^2)} \quad (3)$$

This was employed between computational and experimental $S(Q)$ over the experimental Q range of 1.0 – 23 \AA^{-1} . R was employed due to its popularity in the LEED

community in quantifying the agreement of computational models with experiment. In Fig. S1, the results obtained with R are shown to qualitatively agree with the coefficient of determination in this study.

D. Experimental procedures for creating the LDA “parent” phases.

All uHDA samples, except from uHDA(I_h)*, were prepared in a 0.8 cm diameter pressure die lined with indium, pre-cooled to 77 K, and compressed to 1.6 GPa at 5 kN/min. uHDA(I_h)* was prepared by injecting 0.4 mL H_2O into the pre-cooled indium cup, forming ice I_h , followed by pressure-induced amorphization (PIA) similar to Mishima et al.²² In the case of uHDA from MDA, a 77 K-cooled indium cup was filled with MDA and placed into the pressure die where the preparation of MDA can be found in ref. 66. To create the parent phases of ice I_h and ice I_{sd} , the 0.4 mL H_2O (Milli-Q, Millipore) injected into the cold pressure die was compressed to 0.35 GPa and heated to 200 K forming ice II. Following quenching to 77 K, ice II was decompressed to 100 N whereafter ice I_{sd} or I_h was extracted at 182 K or 260 K, respectively as determined by the in situ volume changes during heating. The resultant ice was then transformed to uHDA through PIA. Further steps were taken when creating eHDA, which was made by heating uHDA to 145 K at 0.25 GPa before quenching to 77 K. All samples were extracted in a liquid nitrogen environment for further analysis.

E. Experimental procedure for transforming LDA samples to ice I_{sd} upon heating.

The various samples were transferred under liquid nitrogen into a purpose-built Kapton window sample holder mounted on a Stoe Stadi P diffractometer with Cu $K\alpha_1$ radiation at 40 kV, 30 mA and monochromated by a Ge 111 crystal. A Mythen 1K area detector collected data every 10 K from 93 – 260 K with a heating rate of 1 K/min as controlled by an Oxford Instruments Cryojet HT. The samples form LDA around 110 K (except ASW and HGW which are already LDA to begin with), and ice I_{sd} around 140 – 150 K, before finally converting to ice I_h above 220 K. An example of this heating procedure when applied to uHDA is shown in Fig. S8. The first ice I_{sd} patterns after the conversion from LDA upon heating were fitted with the MCDIFFaX software.⁹⁶ The software searches for the optimum lattice constants, stacking probabilities, peak profile parameters and zero-shift to reach a χ^2 convergence and hence best-fit to the experimental data. The resultant fits overlaying the experimental data are shown in Fig. S9.

The MCDIFFaX fits of ice I_{sd} from ASW and LDA from ice VIII have already been published in ref. 42 and 97. All other X-ray data has not been previously

published.

V. ACKNOWLEDGEMENTS

We thank S. J. Cox and V. Kapil for stimulating discussions and suggestions, M. Vickers for help with the X-ray diffraction measurements and J. K. Cockcroft for access to a Cryojet HT.

Funding We are grateful to the Materials Chemistry Consortium (Grant EP/L000202) and the UK Materials and Molecular Modelling Hub (Grants EP/P020194/1 and EP/T022213/1) for access to the ARCHER, Thomas, and Young supercomputers. We acknowledge funding from the European Research Council (ERC) under the European Union’s Horizon 2020 research innovation programme grant 725271 and the “n-aqua” ERC project (grant 101071937)).

Competing interests Authors declare that they have no competing interests.

Author contributions

Conceptualization: MBD, CGS, AM.

Investigation: MBD, ARF, CGS, AM.

Funding acquisition: CGS, AM.

Software: MBD, CGS.

Visualisation: MBD, CGS.

Writing – original draft: MBD.

Writing – review & editing: MBD, ARF, CGS, AM.

¹M. Chaplin, “Water structure and science” <https://water.lsbu.ac.uk/>, 2022.

²M. Millot, F. Coppari, J. R. Rygg, A. Correa Barrios, S. Hamel, D. C. Swift, and J. H. Eggert, “Nanosecond X-ray diffraction of shock-compressed superionic water ice,” *Nature*, vol. 569, no. 7755, pp. 251–255, 2019.

³C. G. Salzmann, J. S. Loveday, A. Rosu-Finsen, and C. L. Bull, “Structure and nature of ice XIX,” *Nature communications*, vol. 12, no. 1, pp. 1–7, 2021.

⁴R. Yamane, K. Komatsu, J. Gouchi, Y. Uwatoko, S. Machida, T. Hattori, H. Ito, and H. Kagi, “Experimental evidence for the existence of a second partially-ordered phase of ice VI,” *Nature Communications*, vol. 12, no. 1, p. 1129, 2021.

⁵T. M. Gasser, A. V. Thoeny, A. D. Fortes, and T. Loerting, “Structural characterization of ice XIX as the second polymorph related to ice VI,” *Nature Communications*, vol. 12, no. 1, p. 1128, 2021.

⁶V. B. Prakapenka, N. Holtgrewe, S. S. Lobanov, and A. F. Goncharov, “Structure and properties of two superionic ice phases,” *Nature Physics*, vol. 17, no. 11, pp. 1233–1238, 2021.

⁷C. G. Salzmann, “Advances in the experimental exploration of water’s phase diagram,” *The Journal of chemical physics*, vol. 150, no. 6, p. 60901, 2019.

⁸J. Peter and B. D. F., “Structural Transitions in Amorphous Water Ice and Astrophysical Implications,” *Science*, vol. 265, pp. 753–756, 8 1994.

⁹D. J. Burke and W. A. Brown, “Ice in space: surface science investigations of the thermal desorption of model interstellar ices on dust grain analogue surfaces,” *Phys. Chem. Chem. Phys.*, vol. 12, no. 23, pp. 5947–5969, 2010.

¹⁰P. Ehrenfreund and S. B. Charnley, “Organic molecules in the interstellar medium, comets, and meteorites: a voyage,” *Annu. Rev. Astron. Astrophys.*, vol. 38, pp. 427–483, 2000.

¹¹P. H. Poole, F. Sciortino, U. Essmann, and H. E. Stanley, “Phase behaviour of metastable water,” *Nature*, vol. 360, no. 6402, pp. 324–328, 1992.

¹²O. Mishima and H. E. Stanley, “Decompression-induced melting of ice IV and the liquid–liquid transition in water,” *Nature*, vol. 392, no. 6672, pp. 164–168, 1998.

¹³J. S. Tse, D. D. Klug, C. A. Tulk, I. Swainson, E. C. Svensson, C.-K. Loong, V. Shpakov, V. R. Belosludov, R. V. Belosludov, and Y. Kawazoe, “The mechanisms for pressure-induced amorphization of ice Ih,” *Nature*, vol. 400, no. 6745, pp. 647–649, 1999.

¹⁴H. Schober, M. M. Koza, A. Tölle, C. Masciovecchio, F. Sette, and F. Fujara, “Crystal-like high frequency phonons in the amorphous phases of solid water,” *Physical Review Letters*, vol. 85, no. 19, p. 4100, 2000.

¹⁵P. G. Debenedetti, “Supercooled and glassy water,” *Journal of Physics: Condensed Matter*, vol. 15, no. 45, p. R1669, 2003.

¹⁶B. Geil, M. M. Koza, F. Fujara, H. Schober, and F. Natali, “Absence of fast precursor dynamics of low-density amorphous ice around its hypothetical glass transition temperature,” *Physical Chemistry Chemical Physics*, vol. 6, no. 4, pp. 677–679, 2004.

¹⁷D. T. Limmer and D. Chandler, “Theory of amorphous ices,” *Proceedings of the National Academy of Sciences*, vol. 111, no. 26, pp. 9413–9418, 2014.

¹⁸J. J. Shephard, S. Ling, G. C. Sosso, A. Michaelides, B. Slater, and C. G. Salzmann, “Is high-density amorphous ice simply a “derailed” state along the ice I to ice IV pathway?,” *The Journal of Physical Chemistry Letters*, vol. 8, no. 7, pp. 1645–1650, 2017.

¹⁹P. G. Debenedetti, F. Sciortino, and G. H. Zerze, “Second critical point in two realistic models of water,” *Science*, vol. 369, no. 6501, pp. 289–292, 2020.

²⁰C. A. Tulk, J. J. Molaison, A. R. Makhlufl, C. E. Manning, and D. D. Klug, “Absence of amorphous forms when ice is compressed at low temperature,” *Nature*, vol. 569, no. 7757, pp. 542–545, 2019.

²¹K. H. Kim, K. Amann-Winkel, N. Giovambattista, A. Späh, F. Perakis, H. Pathak, M. L. Parada, C. Yang, D. Mariedahl, T. Eklund, and others, “Experimental observation of the liquid–liquid transition in bulk supercooled water under pressure,” *Science*, vol. 370, no. 6519, pp. 978–982, 2020.

²²O. Mishima, L. D. Calvert, and E. Whalley, “Melting ice I at 77 K and 10 kbar: A new method of making amorphous solids,” *Nature*, vol. 310, no. 5976, pp. 393–395, 1984.

²³J.-C. Li and P. Jenniskens, “Inelastic neutron scattering study of high density amorphous water ice,” *Planetary and space Science*, vol. 45, no. 4, pp. 469–473, 1997.

²⁴O. Andersson and H. Suga, “Thermal conductivity of amorphous ices,” *Physical Review B*, vol. 65, no. 14, p. 140201, 2002.

²⁵O. Andersson and A. Inaba, “Thermal conductivity of crystalline and amorphous ices and its implications on amorphization and glassy water,” *Physical Chemistry Chemical Physics*, vol. 7, no. 7, pp. 1441–1449, 2005.

²⁶O. Andersson, “Dielectric relaxation of low-density amorphous ice under pressure,” *Physical review letters*, vol. 98, no. 5, p. 57602, 2007.

²⁷J. S. Tse, D. M. Shaw, D. D. Klug, S. Patchkovskii, G. Vankó, G. Monaco, and M. Krisch, “X-ray Raman spectroscopic study of water in the condensed phases,” *Physical review letters*, vol. 100, no. 9, p. 95502, 2008.

²⁸M. S. Elsaesser, K. Winkel, E. Mayer, and T. Loerting, “Reversibility and isotope effect of the calorimetric glass→ liquid transition of low-density amorphous ice,” *Physical Chemistry Chemical Physics*, vol. 12, no. 3, pp. 708–712, 2010.

²⁹E. F. Burton and W. F. Oliver, “The crystal structure of ice at low temperatures,” *Proceedings of the Royal Society of London. Series A-Mathematical and Physical Sciences*, vol. 153, no. 878, pp. 166–172, 1935.

³⁰E. F. Burton and W. F. Oliver, “X-ray diffraction patterns of ice,” *Nature*, vol. 135, no. 3413, pp. 505–506, 1935.

³¹P. Brüggegger and E. Mayer, “Complete vitrification in pure liquid

- water and dilute aqueous solutions,” *Nature*, vol. 288, no. 5791, pp. 569–571, 1980.
- ³²E. Mayer and P. Brüggeller, “Vitrification of pure liquid water by high pressure jet freezing,” *Nature*, vol. 298, no. 5876, pp. 715–718, 1982.
- ³³E. Mayer, “New method for vitrifying water and other liquids by rapid cooling of their aerosols,” *Journal of applied physics*, vol. 58, no. 2, pp. 663–667, 1985.
- ³⁴O. Mishima, L. D. Calvert, and E. Whalley, “An apparently first-order transition between two amorphous phases of ice induced by pressure,” *Nature*, vol. 314, no. 6006, pp. 76–78, 1985.
- ³⁵A. Kouchi and T. Kuroda, “Amorphization of cubic ice by ultraviolet irradiation,” *Nature*, vol. 344, no. 6262, pp. 134–135, 1990.
- ³⁶G. A. Baratta, G. Leto, F. Spinella, G. Strazzulla, and G. Foti, “The 3.1 microns feature in ion-irradiated water ice,” *Astronomy and Astrophysics*, vol. 252, pp. 421–424, 1991.
- ³⁷G. Leto and G. A. Baratta, “Ly-alpha photon induced amorphization of Ic water ice at 16 Kelvin-Effects and quantitative comparison with ion irradiation,” *Astronomy & Astrophysics*, vol. 397, no. 1, pp. 7–13, 2003.
- ³⁸D. D. Klug, Y. P. Handa, J. S. Tse, and E. Whalley, “Transformation of ice VIII to amorphous ice by “melting” at low temperature,” *The Journal of Chemical Physics*, vol. 90, pp. 2390–2392, 2 1989.
- ³⁹S. Klotz, J. M. Besson, G. Hamel, R. J. Nelmes, J. S. Loveday, and W. G. Marshall, “Metastable ice VII at low temperature and ambient pressure,” *Nature*, vol. 398, no. 6729, pp. 681–684, 1999.
- ⁴⁰K. Amann-Winkel, R. Böhmer, F. Fujara, C. Gainaru, B. Geil, and T. Loerting, “Colloquium: Water’s controversial glass transitions,” *Reviews of Modern Physics*, vol. 88, no. 1, p. 11002, 2016.
- ⁴¹K. Winkel, D. T. Bowron, T. Loerting, E. Mayer, and J. L. Finney, “Relaxation effects in low density amorphous ice: Two distinct structural states observed by neutron diffraction,” *The Journal of chemical physics*, vol. 130, no. 20, p. 204502, 2009.
- ⁴²J. J. Shephard, S. Klotz, M. Vickers, and C. G. Salzmänn, “A new structural relaxation pathway of low-density amorphous ice,” *The Journal of Chemical Physics*, vol. 144, no. 20, p. 204502, 2016.
- ⁴³J. L. Finney, A. Hallbrucker, I. Kohl, A. K. Soper, and D. T. Bowron, “Structures of high and low density amorphous ice by neutron diffraction,” *Physical review letters*, vol. 88, no. 22, p. 225503, 2002.
- ⁴⁴D. Mariedahl, F. Perakis, A. Späh, H. Pathak, K. H. Kim, G. Camisasca, D. Schlesinger, C. Benmore, L. G. M. Pettersson, A. Nilsson, and others, “X-ray scattering and O–O pair-distribution functions of amorphous ices,” *The Journal of Physical Chemistry B*, vol. 122, no. 30, pp. 7616–7624, 2018.
- ⁴⁵F. Martelli, N. Giovambattista, S. Torquato, and R. Car, “Searching for crystal-ice domains in amorphous ices,” *Physical Review Materials*, vol. 2, no. 7, p. 75601, 2018.
- ⁴⁶F. Martelli, S. Torquato, N. Giovambattista, and R. Car, “Large-scale structure and hyperuniformity of amorphous ices,” *Physical review letters*, vol. 119, no. 13, p. 136002, 2017.
- ⁴⁷N. Giovambattista, C. A. Angell, F. Sciortino, and H. E. Stanley, “Glass-transition temperature of water: a simulation study,” *Physical review letters*, vol. 93, no. 4, p. 47801, 2004.
- ⁴⁸N. Giovambattista, H. E. Stanley, and F. Sciortino, “Cooling rate, heating rate, and aging effects in glassy water,” *Physical Review E*, vol. 69, no. 5, p. 50201, 2004.
- ⁴⁹N. Giovambattista, P. G. Debenedetti, F. Sciortino, and H. E. Stanley, “Structural order in glassy water,” *Physical Review E*, vol. 71, no. 6, p. 61505, 2005.
- ⁵⁰T. E. Gartner, S. Torquato, R. Car, and P. G. Debenedetti, “Manifestations of metastable criticality in the long-range structure of model water glasses,” *Nature Communications*, vol. 12, no. 1, p. 3398, 2021.
- ⁵¹N. Giovambattista, H. E. Stanley, and F. Sciortino, “Potential-energy landscape study of the amorphous-amorphous transformation in H₂O,” *Physical review letters*, vol. 91, no. 11, p. 115504, 2003.
- ⁵²M. Formanek, S. Torquato, R. Car, and F. Martelli, “Molecular Rotations, Multiscale Order, Hyperuniformity, and Signatures of Metastability during the Compression/Decompression Cycles of Amorphous Ices,” *The Journal of Physical Chemistry B*, 4 2023.
- ⁵³B. Guillot and Y. Guissani, “Polyamorphism in low temperature water: A simulation study,” *The Journal of chemical physics*, vol. 119, no. 22, pp. 11740–11752, 2003.
- ⁵⁴D. Mariedahl, F. Perakis, A. Späh, H. Pathak, K. H. Kim, C. Benmore, A. Nilsson, and K. Amann-Winkel, “X-ray studies of the transformation from high- to low-density amorphous water,” *Philosophical Transactions of the Royal Society A*, vol. 377, no. 2146, p. 20180164, 2019.
- ⁵⁵V. Molinero and E. B. Moore, “Water Modeled As an Intermediate Element between Carbon and Silicon,” *The Journal of Physical Chemistry B*, vol. 113, pp. 4008–4016, 4 2009.
- ⁵⁶M. Seidl, K. Amann-Winkel, P. H. Handle, G. Zifferer, and T. Loerting, “From parallel to single crystallization kinetics in high-density amorphous ice,” *Physical Review B*, vol. 88, no. 17, p. 174105, 2013.
- ⁵⁷T. L. Malkin, B. J. Murray, A. V. Brukhno, J. Anwar, and C. G. Salzmänn, “Structure of ice crystallized from supercooled water,” *Proceedings of the National Academy of Sciences*, vol. 109, pp. 1041–1045, 1 2012.
- ⁵⁸E. B. Moore and V. Molinero, “Is it cubic? Ice crystallization from deeply supercooled water,” *Physical Chemistry Chemical Physics*, vol. 13, no. 44, p. 20008, 2011.
- ⁵⁹A. Haji-Akbari and P. G. Debenedetti, “Direct calculation of ice homogeneous nucleation rate for a molecular model of water,” *Proceedings of the National Academy of Sciences*, vol. 112, pp. 10582–10588, 8 2015.
- ⁶⁰L. Lupi, A. Hudait, B. Peters, M. Grünwald, R. Gotchy Mullen, A. H. Nguyen, and V. Molinero, “Role of stacking disorder in ice nucleation,” *Nature*, vol. 551, no. 7679, pp. 218–222, 2017.
- ⁶¹M. B. Davies, M. Fitzner, and A. Michaelides, “Routes to cubic ice through heterogeneous nucleation,” *Proceedings of the National Academy of Sciences*, vol. 118, p. e2025245118, 3 2021.
- ⁶²J. B. Pendry, “Reliability factors for LEED calculations,” *Journal of Physics C: Solid State Physics*, vol. 13, no. 5, pp. 937–944, 1980.
- ⁶³E. Zanazzi and F. Jona, “A reliability factor for surface structure determinations by low-energy electron diffraction,” *Surface Science*, vol. 62, no. 1, pp. 61–80, 1977.
- ⁶⁴J. J. Shephard, J. S. O. Evans, and C. G. Salzmänn, “Structural relaxation of low-density amorphous ice upon thermal annealing,” *The Journal of Physical Chemistry Letters*, vol. 4, no. 21, pp. 3672–3676, 2013.
- ⁶⁵J. L. F. Abascal and C. Vega, “A general purpose model for the condensed phases of water: TIP4P/2005,” *The Journal of Chemical Physics*, vol. 123, p. 234505, 12 2005.
- ⁶⁶A. Rosu-Finsen, M. B. Davies, A. Amon, H. Wu, A. Sella, A. Michaelides, and C. G. Salzmänn, “Medium-density amorphous ice,” *Science*, vol. 379, pp. 474–478, 2 2023.
- ⁶⁷I. Kohl, E. Mayer, and A. Hallbrucker, “The glassy water–cubic ice system: a comparative study by X-ray diffraction and differential scanning calorimetry,” *Physical Chemistry Chemical Physics*, vol. 2, no. 8, pp. 1579–1586, 2000.
- ⁶⁸T. H. G. Carr, J. J. Shephard, and C. G. Salzmänn, “Spectroscopic Signature of Stacking Disorder in Ice I,” *The Journal of Physical Chemistry Letters*, vol. 5, pp. 2469–2473, 7 2014.
- ⁶⁹J. Huebinger, H.-M. Han, O. Hofnagel, I. R. Vetter, P. I. H. Bastiaens, and M. Grabenbauer, “Direct Measurement of Water States in Cryopreserved Cells Reveals Tolerance toward Ice Crystallization,” *Biophysical journal*, vol. 110, pp. 840–849, 2 2016.
- ⁷⁰K. A. Murray and M. I. Gibson, “Chemical approaches to cryopreservation,” *Nature Reviews Chemistry*, vol. 6, no. 8, pp. 579–593, 2022.
- ⁷¹D. Cressey and E. Callaway, “Cryo-electron microscopy wins

- chemistry Nobel,” *Nature*, vol. 550, no. 7675, p. 167, 2017.
- ⁷²M. D. Ediger, “Perspective: Highly stable vapor-deposited glasses,” *The Journal of chemical physics*, vol. 147, no. 21, p. 210901, 2017.
- ⁷³M. L. Rudee and A. Howie, “The structure of amorphous Si and Ge,” *The Philosophical Magazine: A Journal of Theoretical Experimental and Applied Physics*, vol. 25, pp. 1001–1007, 4 1972.
- ⁷⁴M. M. J. Treacy and K. B. Borisenko, “The local structure of amorphous silicon,” *Science*, vol. 335, no. 6071, pp. 950–953, 2012.
- ⁷⁵S. F. Swallen, K. L. Kearns, M. K. Mapes, Y. S. Kim, R. J. McMahon, M. D. Ediger, T. Wu, L. Yu, and S. Satija, “Organic glasses with exceptional thermodynamic and kinetic stability,” *Science*, vol. 315, no. 5810, pp. 353–356, 2007.
- ⁷⁶W. Kauzmann, “The nature of the glassy state and the behavior of liquids at low temperatures,” *Chemical reviews*, vol. 43, no. 2, pp. 219–256, 1948.
- ⁷⁷S. Plimpton, “Fast Parallel Algorithms for Short-Range Molecular Dynamics,” *Journal of Computational Physics*, vol. 117, no. 1, pp. 1–19, 1995.
- ⁷⁸T. Li, D. Donadio, G. Russo, and G. Galli, “Homogeneous ice nucleation from supercooled water,” *Physical Chemistry Chemical Physics*, vol. 13, no. 44, pp. 19807–19813, 2011.
- ⁷⁹T. Li, D. Donadio, and G. Galli, “Ice nucleation at the nanoscale probes no man’s land of water,” *Nature Communications*, vol. 4, no. 1, p. 1887, 2013.
- ⁸⁰L. Lupi, A. Hudait, and V. Molinero, “Heterogeneous Nucleation of Ice on Carbon Surfaces,” *Journal of the American Chemical Society*, vol. 136, pp. 3156–3164, 2 2014.
- ⁸¹G. C. Sosso, J. Chen, S. J. Cox, M. Fitzner, P. Pedevilla, A. Zen, and A. Michaelides, “Crystal Nucleation in Liquids: Open Questions and Future Challenges in Molecular Dynamics Simulations,” *Chemical Reviews*, vol. 116, no. 12, pp. 7078–7116, 2016.
- ⁸²M. Fitzner, G. C. Sosso, S. J. Cox, and A. Michaelides, “The Many Faces of Heterogeneous Ice Nucleation: Interplay between Surface Morphology and Hydrophobicity,” *Journal of the American Chemical Society*, vol. 137, no. 42, pp. 13658–13669, 2015.
- ⁸³M. B. Davies, M. Fitzner, and A. Michaelides, “Accurate prediction of ice nucleation from room temperature water,” *Proceedings of the National Academy of Sciences*, vol. 119, no. 31, p. e2205347119, 2022.
- ⁸⁴D. Quigley, “Communication: Thermodynamics of stacking disorder in ice nuclei,” *The Journal of Chemical Physics*, vol. 141, p. 121101, 9 2014.
- ⁸⁵A. Hudait, S. Qiu, L. Lupi, and V. Molinero, “Free energy contributions and structural characterization of stacking disordered ices,” *Phys. Chem. Chem. Phys.*, vol. 18, no. 14, pp. 9544–9553, 2016.
- ⁸⁶T. Hondoh, T. Itoh, S. Amakai, K. Goto, and A. Higashi, “Formation and annihilation of stacking faults in pure ice,” *The Journal of Physical Chemistry*, vol. 87, pp. 4040–4044, 10 1983.
- ⁸⁷C. Vega and J. L. F. Abascal, “Relation between the melting temperature and the temperature of maximum density for the most common models of water,” *The Journal of Chemical Physics*, vol. 123, p. 144504, 10 2005.
- ⁸⁸H. Y. Playford, T. F. Whale, B. J. Murray, M. G. Tucker, and C. G. Salzmann, “Analysis of stacking disorder in ice I using pair distribution functions,” *Journal of Applied Crystallography*, vol. 51, no. 4, pp. 1211–1220, 2018.
- ⁸⁹S. Le Roux and P. Jund, “Ring statistics analysis of topological networks: New approach and application to amorphous GeS₂ and SiO₂ systems,” *Computational Materials Science*, vol. 49, no. 1, pp. 70–83, 2010.
- ⁹⁰W. Humphrey, A. Dalke, and K. Schulten, “VMD - Visual Molecular Dynamics,” *Journal of Molecular Graphics*, vol. 14, pp. 33–38, 1996.
- ⁹¹J. Stone, *An Efficient Library for Parallel Ray Tracing and Animation*. PhD thesis, Computer Science Department, University of Missouri-Rolla, 4 1998.
- ⁹²J. R. Espinosa, C. Vega, C. Valeriani, and E. Sanz, “Seeding approach to crystal nucleation,” *The Journal of Chemical Physics*, vol. 144, p. 34501, 1 2016.
- ⁹³W. Lechner and C. Dellago, “Accurate determination of crystal structures based on averaged local bond order parameters,” *The Journal of Chemical Physics*, vol. 129, p. 114707, 9 2008.
- ⁹⁴M. Bonomi, D. Branduardi, G. Bussi, C. Camilloni, D. Provasi, P. Raiteri, D. Donadio, F. Marinelli, F. Pietrucci, R. A. Broglia, and M. Parrinello, “PLUMED: A portable plugin for free-energy calculations with molecular dynamics,” *Computer Physics Communications*, vol. 180, no. 10, pp. 1961–1972, 2009.
- ⁹⁵G. A. Tribello, M. Bonomi, D. Branduardi, C. Camilloni, and G. Bussi, “PLUMED 2: New feathers for an old bird,” *Computer Physics Communications*, vol. 185, no. 2, pp. 604–613, 2014.
- ⁹⁶C. G. Salzmann, B. J. Murray, and J. J. Shephard, “Extent of stacking disorder in diamond,” *Diamond and Related Materials*, vol. 59, pp. 69–72, 2015.
- ⁹⁷A. Rosu-Finsen, B. Chikani, and C. G. Salzmann, “Thermal Desorption of H₂O-Ice: From Nanoscale Films to the Bulk,” 2022.

Supporting Materials for How Crystalline is Low Density Amorphous Ice?

Michael Benedict Davies,^{1,2} Alexander Rosu-Finsen,³ Christoph G. Salzmann,^{3, a)} and
Angelos Michaelides^{2, 1, b)}

¹⁾*Department of Physics and Astronomy, University College London, WC1E 6BT, UK.*

²⁾*Yusuf Hamied Department of Chemistry, University of Cambridge, Lensfield Road, Cambridge CB2 1EW, UK.*

³⁾*Department of Chemistry, University College London, 20 Gordon Street, London WC1H 0AJ, UK.*

^{a)}Electronic mail: c.salzmann@ucl.ac.uk

^{b)}Electronic mail: am452@cam.ac.uk

CONTENTS

S1. Supplementary Text	S3
A. Finite size effect when quenching liquid water	S3
B. Differences between LDA models from quenching liquid water and from polycrystalline ice	S3
C. Primitive ring distributions of liquid water, ice I_h , and the LDA models obtained in simulation	S4
D. Experiments on obtaining I_{sd} from LDA	S4
S2. Supplementary Figures	S5
References	S18

S1. SUPPLEMENTARY TEXT

A. Finite size effect when quenching liquid water

Fig. S1 compares the results of quenching a large system with 192,000 mW molecules (as presented in the main manuscript), to a smaller 3,000 mW molecule system. A clear difference in behaviour is observed which can be explained by the nucleation rates dependence on volume. This volume dependence means that for the smaller system such an optimal match to LDA is not found. The system volume is too small to statistically see multiple local homogeneous nucleation events. Thus the LDA structure with the optimal balance of heterogeneity at small scales (due to the presence of crystalline grains) but isotropy at large scales (due to the random orientation, location, and size of the grains) is not achieved.

B. Differences between LDA models from quenching liquid water and from polycrystalline ice

There is a slightly higher crystallinity for the LDA model found from the polycrystalline (25 %) versus the quenched systems (19 %). This difference is due to different distribution of crystalline ice grains in each model. Quenching produces crystalline ice through homogeneous ice nucleation, which is a stochastic process. The polycrystalline structures are similarly built in a stochastic manner, having defined numbers of randomly positioned and orientated nucleation sites which then grow isotropically at the same speed until they impinge on the neighbouring domains. However, the resulting grains of crystalline ice are more uniform in size than achieved through quenching. For randomly orientated grains, a small number of large grains gives a more structured $S(Q)$ than the same amount of ice broken into many smaller domains. This results in the relatively small difference in crystallinity observed between the two LDA models, which can be taken as approximate upper and lower bounds for the crystallinity of experimental LDA. We also note that there is a slight difference in cubicity (48 % and 33 %) of the crystalline grains in the two LDA models; however the two lie within the optimal cubicity indicated by the polycrystalline structures (25 – 50 %).

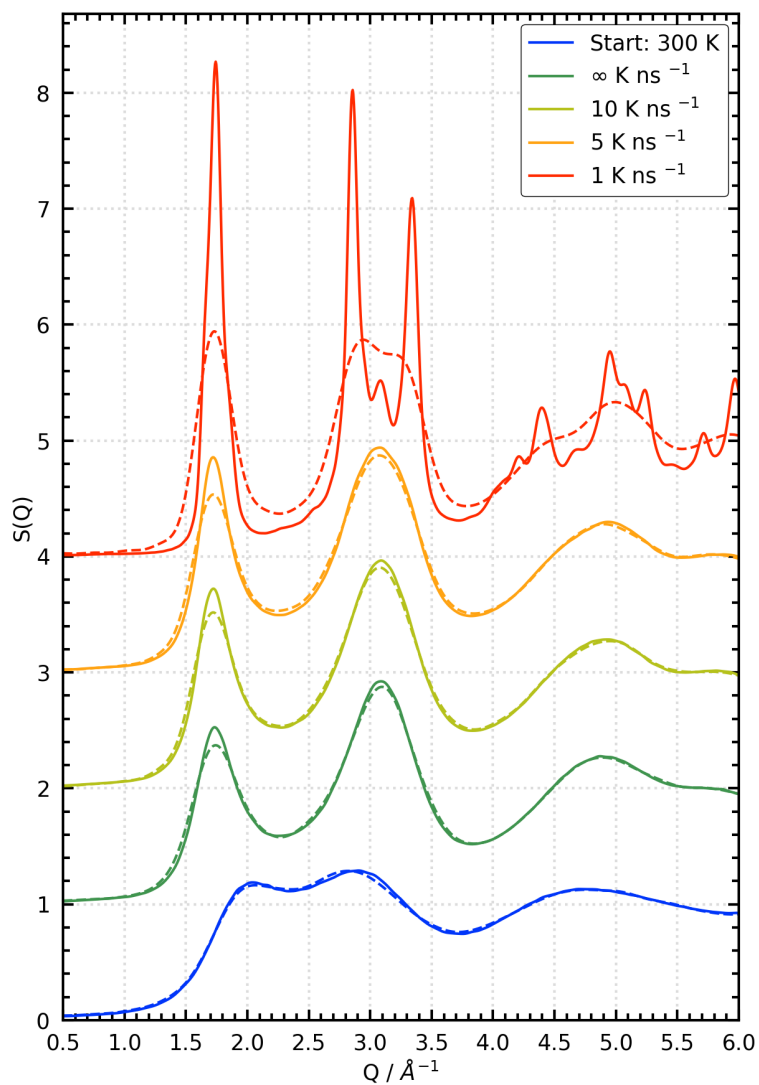
C. Primitive ring distributions of liquid water, ice I_h, and the LDA models obtained in simulation

Fig. S6 shows the primitive ring distributions of the structures. Both LDA models are very similar, peaking at 6-membered rings (which ice I is entirely comprised of), along with a significant number of 5- and 7-membered rings. Physically, this is consistent with a partially crystallised state: similar distributions have been reported by Haji-Akbari and Debendetti for ice nuclei formed in homogeneous nucleation, and by Fitzner et al. for the most immobile regions of supercooled water where homogeneous nucleation was found to occur.^{1,2}

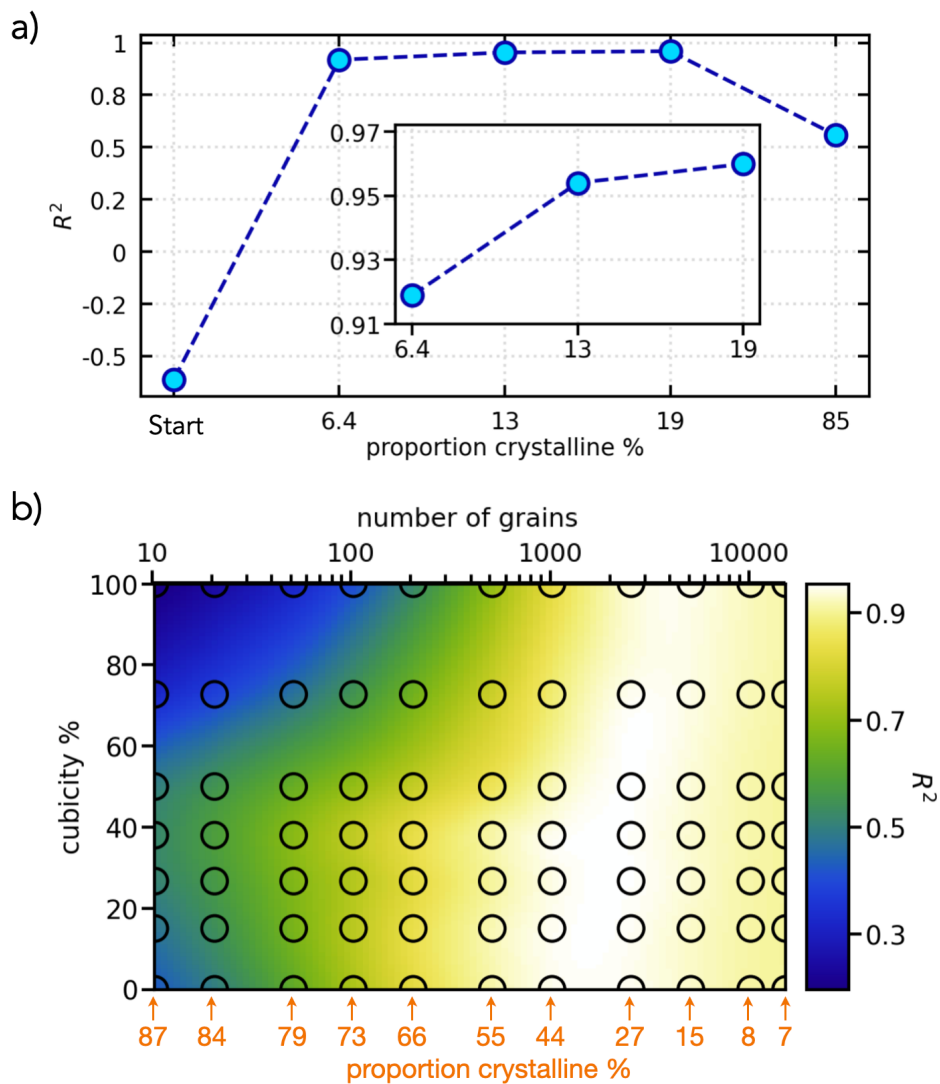
D. Experiments on obtaining I_{sd} from LDA

The parent phase of LDA is either a different type of ice or the LDA has been prepared through different routes. The LDA is then heated to obtain ice I_{sd} while XRD patterns are recorded. The heating rates are the same for all data sets. As seen in Table S1, LDA as well as ice IX are formed when heating ice VIII. However, the amount of ice IX formed has previously been estimated to be at most 5 %, ³ and therefore deemed to have a minor effect on the resultant ice I_{sd} diffraction pattern upon further heating.

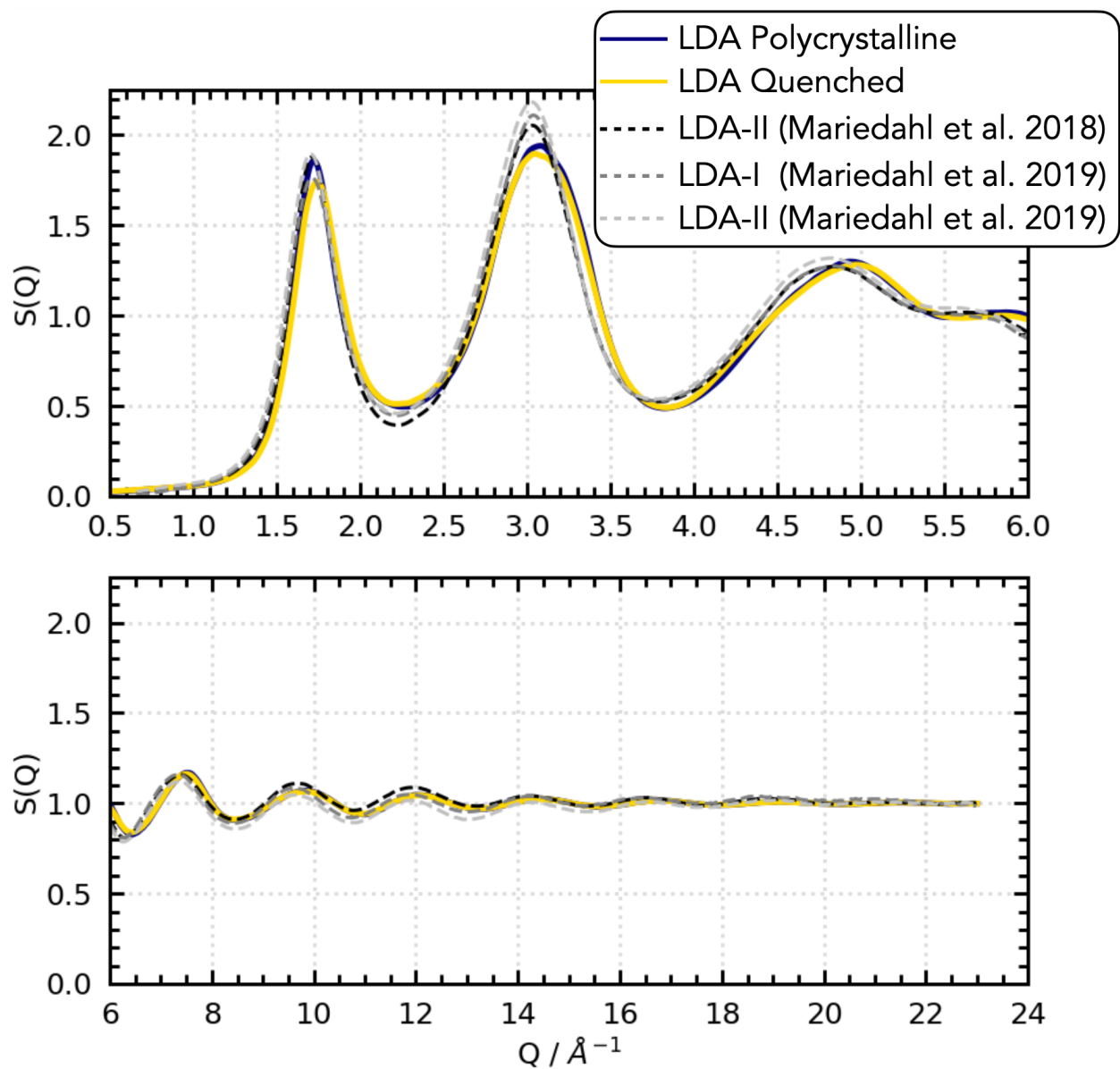
S2. SUPPLEMENTARY FIGURES



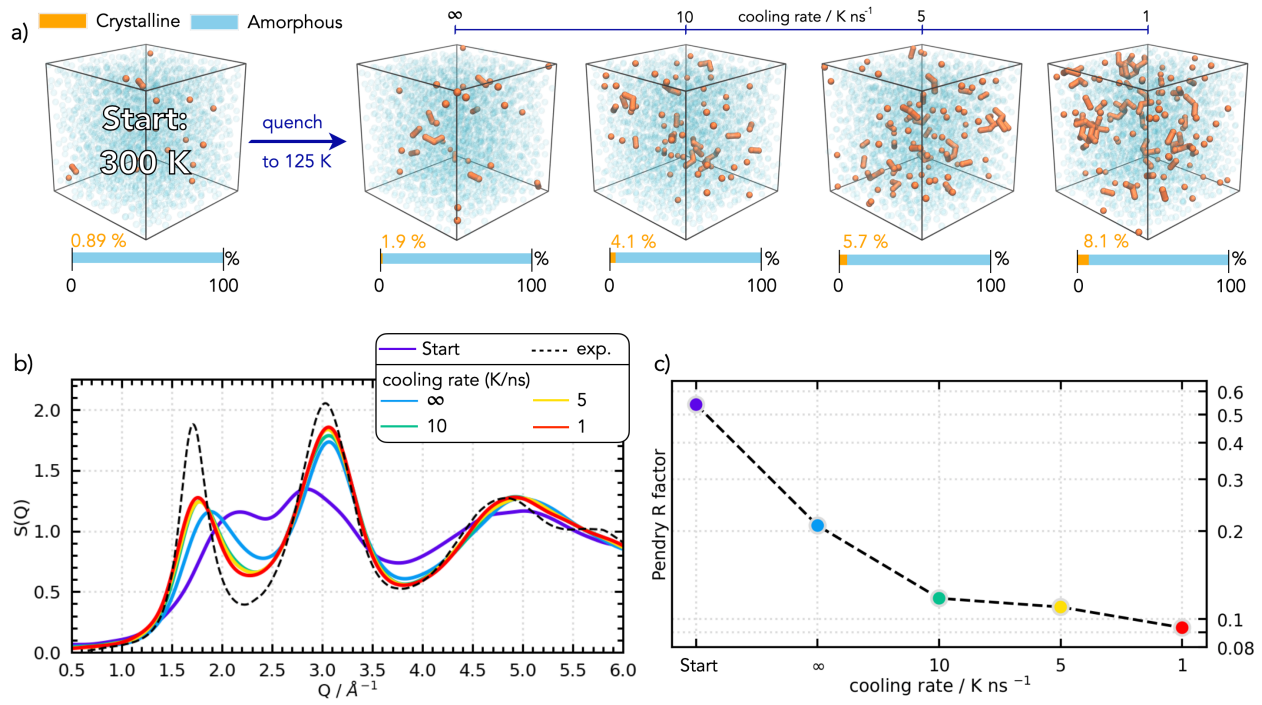
Supplementary Figure S1. A finite size effect when quenching liquid water in simulation. $S(Q)$ of approximately $21 \times 21 \times 21$ nm periodic simulation box with 192,000 mW molecules (solid lines) versus approximately $4 \times 4 \times 4$ nm periodic simulation box with 3,000 mW molecules (dashed lines).



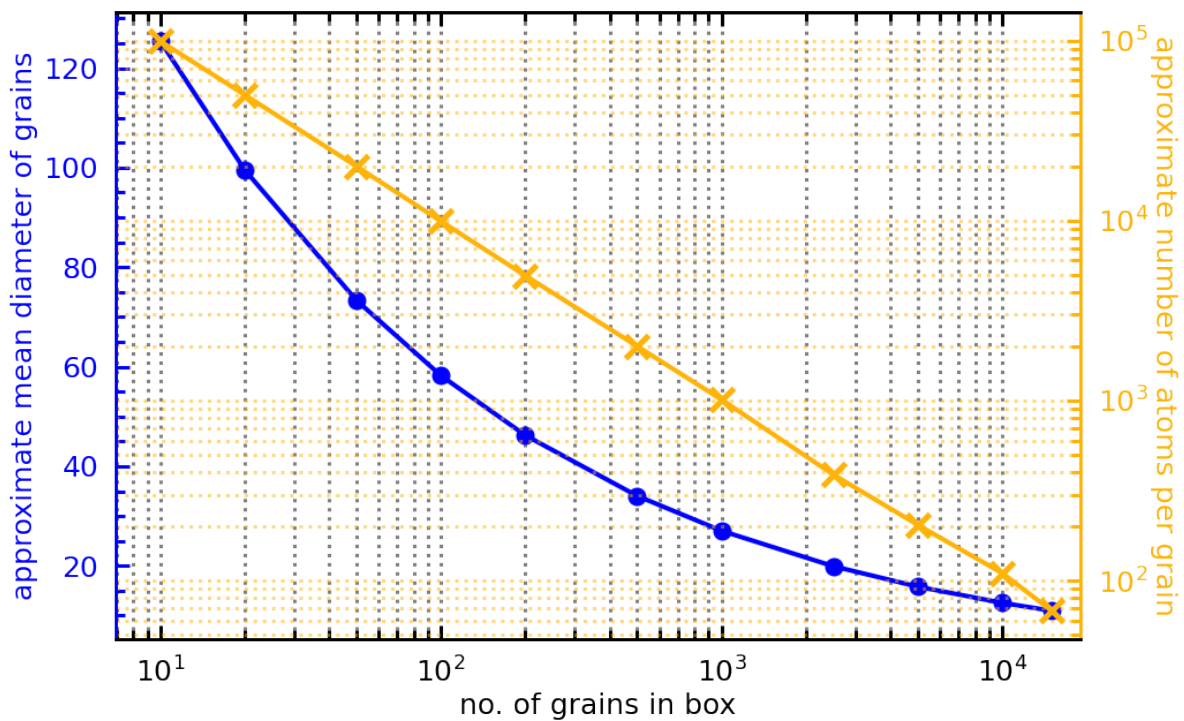
Supplementary Figure S2. Agreement between $S(Q)$ of computational models and experiment for LDA (LDA-II of Mariedahl et al.⁴) as quantified by the coefficient of determination (R^2). A negative R^2 is achieved if a fit is worse than a horizontal line at the mean of the data. (a) Structural models from quenching liquid water. (b) Structural models from building polycrystalline ice. Please note that R^2 is not the square of the Pendry R factor.



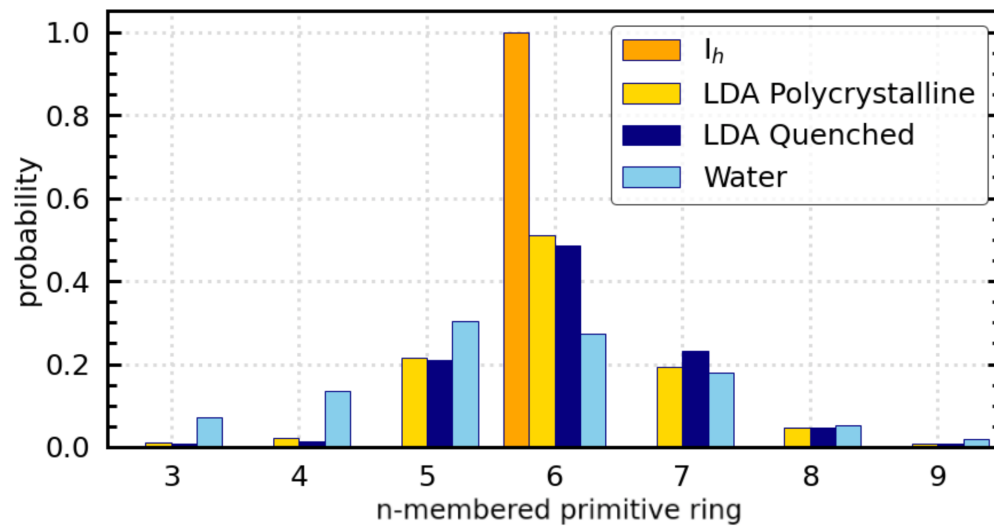
Supplementary Figure S3. Experimental $S(Q)$ of LDA-I and LDA-II measured by Mariedahl et al. (2019)⁵ are plotted with the experimental LDA-II pattern of Mariedahl et al. (2018)⁴ used in the main manuscript and the two optimal computational LDA models discovered in this study.



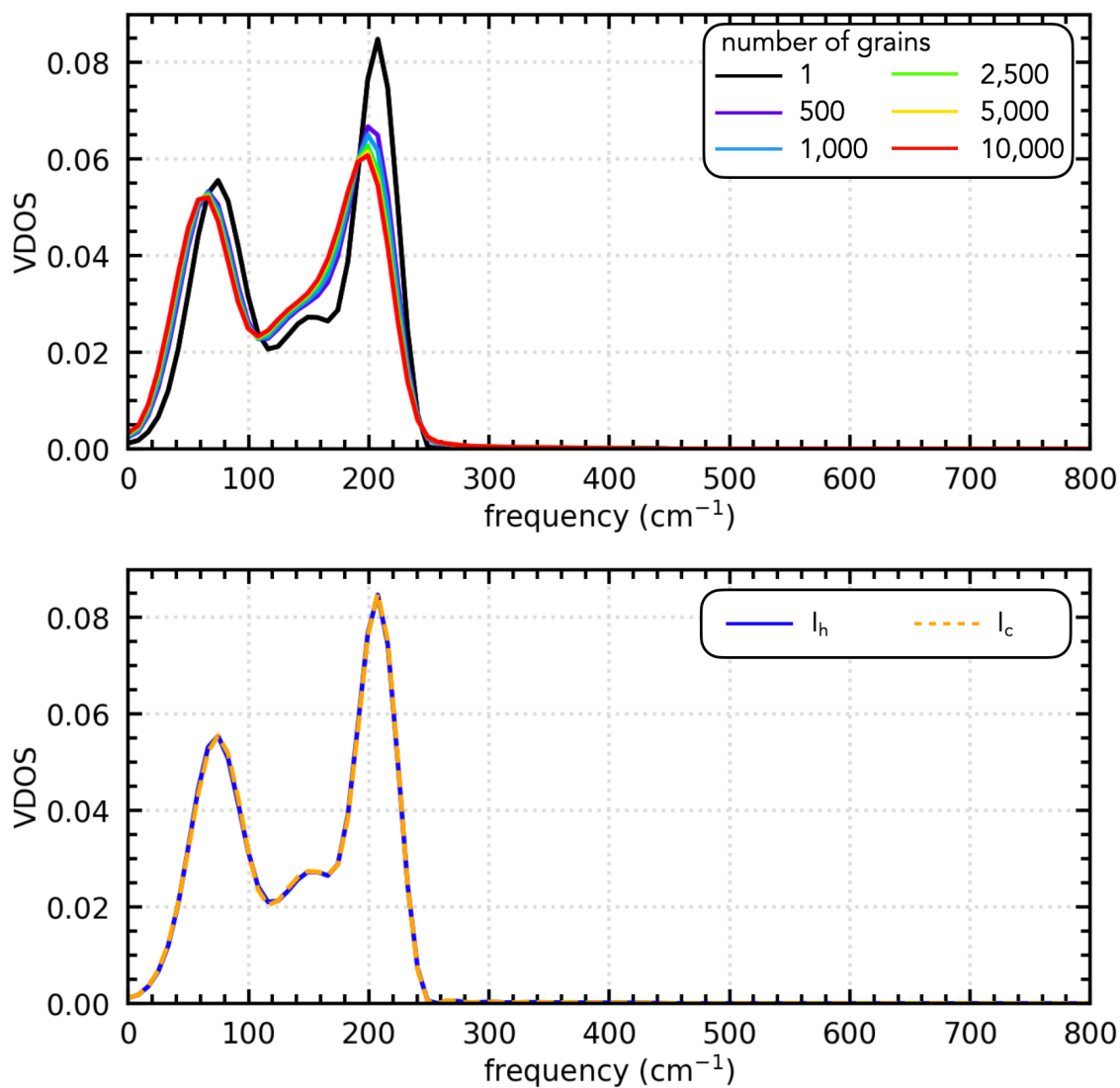
Supplementary Figure S4. Quenching liquid water using the TIP4P/2005 water model. (a) Snapshots of systems taken from quenching water from 300 K to 125 K at different cooling rates. (b) $S(Q)$ of quenched systems along with experiment (black dashed line). (c) Pendry R factor against cooling rate for TIP4P/2005.



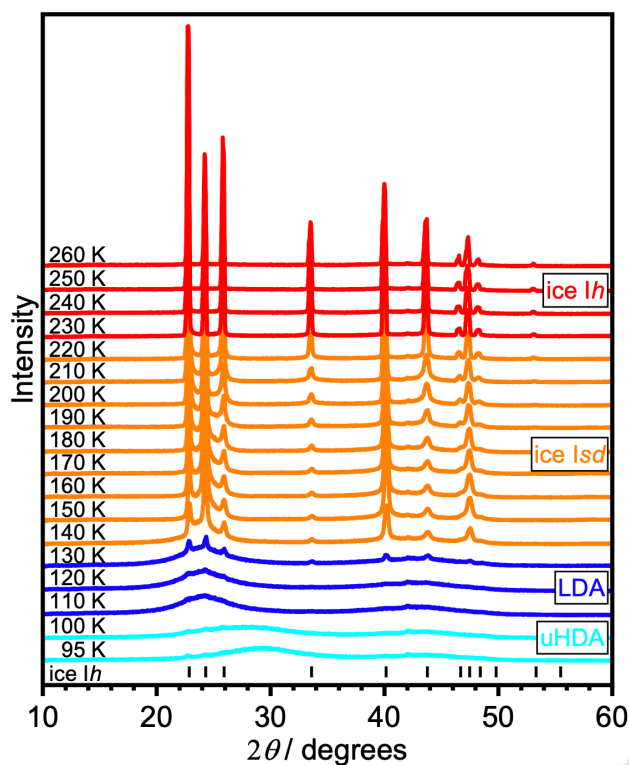
Supplementary Figure S5. Approximate mean diameter of ice grains (blue) and the approximate number of atoms per grain (orange) from the computational polycrystalline systems. Diameters are calculated by assuming that the grains are spherical, and equating their cumulative volume to the volume of the system. The number of atoms per grain is taken by cutting a sphere with the corresponding diameter from an ice I_h structure at 0 K.



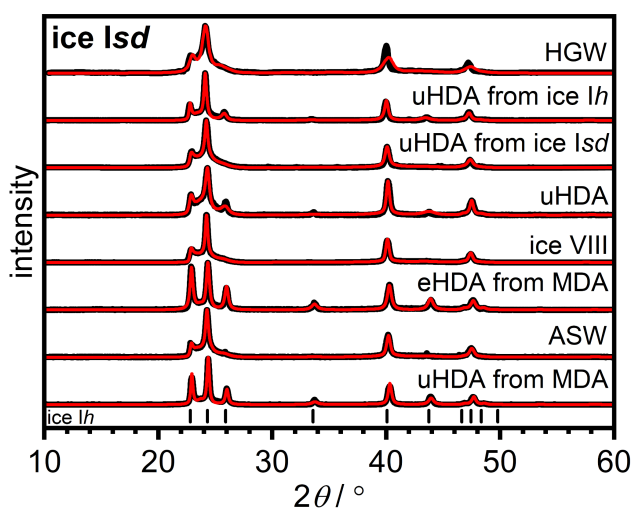
Supplementary Figure S6. Primitive ring distributions of liquid water, ice I_h , and the LDA models obtained in simulation. We note, ice I_h , ice I_c and ice I_{sd} are all comprised entirely of six-membered rings.



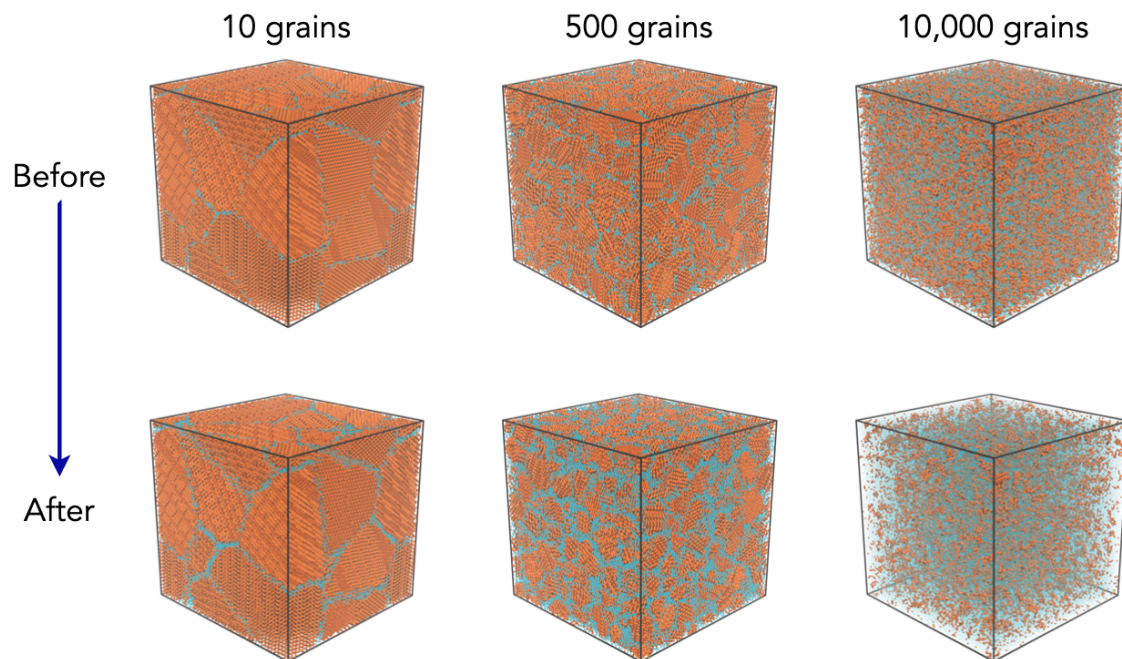
Supplementary Figure S7. Comparison of vibrational density of states (VDOS) for bulk and polycrystalline computational systems. (top) VDOS for different levels of polycrystallinity of ice at 38 % cubicity; one grain refers to the bulk structure. (bottom) VDOS for bulk ice I_h and ice I_c.



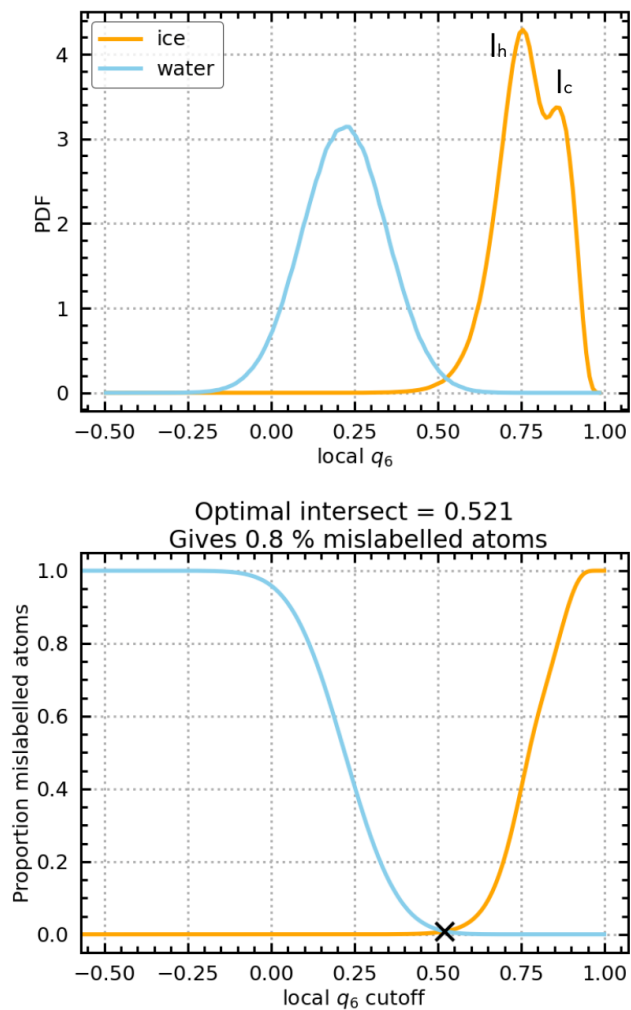
Supplementary Figure S8. Entire progression upon heating uHDA (cyan) in experiment, which transforms to LDA (blue) around 110 K, to ice I_{sd} near 140-150 K and finally to ice I_h near 220-230 K.



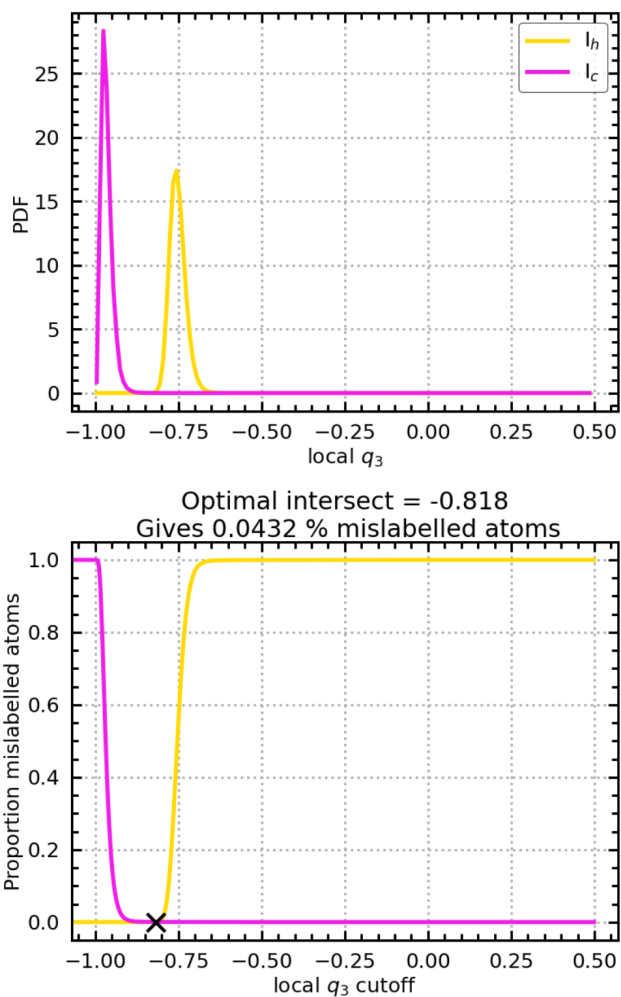
Supplementary Figure S9. Experimental ice I_{sd} X-ray diffraction patterns immediately after the transition from LDA (black) and the corresponding MCDIFFaX fits (red).



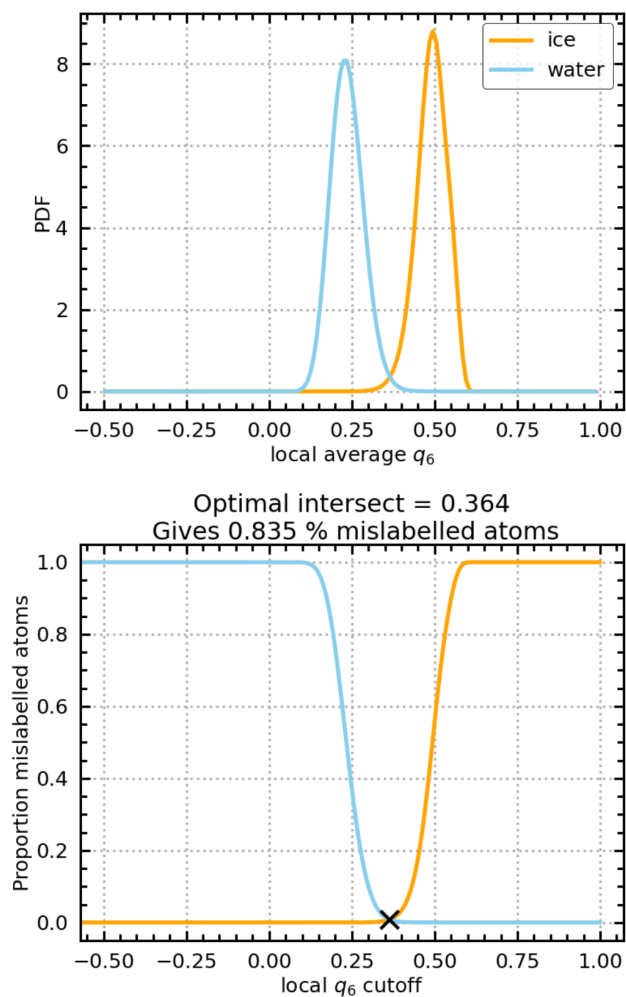
Supplementary Figure S10. Snapshots of the structures of the computational polycrystalline systems before and after annealing.



Supplementary Figure S11. Procedure to identify molecules with crystalline and amorphous local environments using the mW water model. (top) Distributions of local q_6 for water and ice. Distribution for ice comes from combining local q_6 from the bulk ice I_h and ice I_c simulations. (bottom) Proportion of mislabelled atoms for different choices of the local q_6 cutoff between crystalline and amorphous environments.



Supplementary Figure S12. Procedure to identify molecules with cubic and hexagonal local environments for the mW water model. (top) Distributions of local q_3 for ice I_h and ice I_c . (bottom) Proportion of mislabelled atoms for different choices of the local q_6 cutoff between ice I_h and ice I_c environments.



Supplementary Figure S13. Procedure to identify molecules with crystalline and amorphous local environments for the TIP4P/2005 water model. (top) Distributions of local q_6 for water and ice. Distribution for ice comes from combining local q_6 from the bulk ice I_h and ice I_c simulations. (bottom) Proportion of mislabelled atoms for different choices of the local q_6 cutoff between crystalline and amorphous environments.

TABLE S1. Transition of phases for converting LDA samples to ice I_{sd} in experiment. (*) Both ice I_h and ice I_{sd} were made in the press by first making ice II, removing the force to 100 N, and heating to beyond the transitions to ice I_h or ice I_{sd} before quenching and recompression to uHDA.

Parent ice	Intermediate ice upon heating	Final product upon heating
MDA compressed to uHDA	LDA	ice I_{sd} and then ice I_h
uHDA	LDA	ice I_{sd} and then ice I_h
ice I_h compressed to uHDA*	LDA	ice I_{sd} and then ice I_h
ice I_{sd} compressed to uHDA*	LDA	ice I_{sd} and then ice I_h
MDA compressed to eHDA	LDA	ice I_{sd} and then ice I_h
Ice VIII	LDA & ice IX	ice I_{sd} and then ice I_h
ASW/LDA	n/a	ice I_{sd} and then ice I_h
HGW/LDA	n/a	ice I_{sd} and then ice I_h

REFERENCES

- ¹A. Haji-Akbari and P. G. Debenedetti, “Direct calculation of ice homogeneous nucleation rate for a molecular model of water,” *Proceedings of the National Academy of Sciences*, vol. 112, pp. 10582–10588, 8 2015.
- ²M. Fitzner, G. C. Sosso, S. J. Cox, and A. Michaelides, “Ice is born in low-mobility regions of supercooled liquid water,” *Proceedings of the National Academy of Sciences*, vol. 116, pp. 2009–2014, 2 2019.
- ³J. J. Shephard, S. Klotz, M. Vickers, and C. G. Salzmann, “A new structural relaxation pathway of low-density amorphous ice,” *The Journal of Chemical Physics*, vol. 144, no. 20, p. 204502, 2016.
- ⁴D. Mariedahl, F. Perakis, A. Späh, H. Pathak, K. H. Kim, G. Camisasca, D. Schlesinger, C. Benmore, L. G. M. Pettersson, A. Nilsson, and others, “X-ray scattering and O–O pair-distribution functions of amorphous ices,” *The Journal of Physical Chemistry B*, vol. 122, no. 30, pp. 7616–7624, 2018.
- ⁵D. Mariedahl, F. Perakis, A. Späh, H. Pathak, K. H. Kim, C. Benmore, A. Nilsson, and K. Amann-Winkel, “X-ray studies of the transformation from high-to low-density amorphous water,” *Philosophical Transactions of the Royal Society A*, vol. 377, no. 2146, p. 20180164, 2019.